Marine and Petroleum Geology 129 (2021) 105082

Contents lists available at ScienceDirect

Marine and Petroleum Geology

journal homepage: www.elsevier.com/locate/marpetgeo

Diagenesis of the Malmian Mikulov Formation source rock, Vienna Basin: Focus on matrix and pores

Andrea Schicker [a], Susanne Gier [a,*], Jürgen Schieber [b], Peter Krois [c]

[a] Department of Geodynamics and Sedimentology, University of Vienna, Althanstrasse 14, 1090, Vienna, Austria
[b] Department of Geological Sciences, Indiana University, 1001 East 10th Street, Bloomington, IN, 47405-1405, USA
[c] OMV Exploration & Production, Trabrennstrasse 6-8, 1020, Vienna, Austria

ARTICLE INFO

Keywords:
Clay mineralogy
Diagenesis
Illite-smectite
Mudstone matrix
Mikulov formation
Shale gas
Vienna basin

ABSTRACT

Diagenetic processes and pore development in the matrix of the 1000 m thick main source rock for oil and gas in the Vienna Basin, the autochthonous Malmian mudstones of the Mikulov Formation have been studied. Core samples from wells over a true vertical depth range of 1400 m–8551 m were available. The bulk samples contain quartz, minor amounts of plagioclase, pyrite and a large but variable proportion of calcite; the clay mineral content ranges from 14 to 47%. The clay fraction contains a prominent illite-smectite (I–S) mixed-layer phase, illite, chlorite and kaolinite. The quantities of I–S and kaolinite decrease with depth, whereas illite and chlorite increase with depth. Diagenesis has involved a gradual transformation of smectite to illite through mixed-layer I–S intermediates. The ordering of the mixed layer I–S changes with increasing depth from R0 to R1 and R3. The R1 transformation of the mixed-layer I–S occurs at approximately 3000 m and vitrinite reflectance values of 0.4%–0.6%. Based on petrographic evidence, the cations resulting from the illitization of smectite were the source of a variety of late diagenetic mineral cements, such as Fe and Mg for chlorite formation and for ferroan dolomite precipitation. Illitization also provided Si for local quartz cementation. During diagenesis nanometer to micrometer size pores developed because of specific mineral frameworks and dissolution processes. Organic matter pores developed in deeper, thermally mature samples. Phyllosilicate framework pores between brittle grains are commonly observed. Pores caused by partial dissolution of carbonate grains also occur. In places diagenetic cements, such as quartz overgrowths or carbonate cements keep pores propped open. The connectivity of the pores cannot be established unequivocally from SEM photomicrographs, but they likely contribute to the creation and preservation of effective porosity and gas storage capacity of these rocks.

1. Introduction

Most publications about the diagenesis of mudstones focus on the detrital silt-sized minerals like quartz, feldspars, carbonates and the cementation related to them (Day-Stirrat et al., 2010; Dowey and Taylor, 2017, 2019), whereas statements about the diagenesis of the finer grained matrix are comparatively more speculative. The most common matrix components are clay minerals such as smectite, illite, kaolinite and chlorite together with Fe-minerals and organic matter. Pure smectite characterizes the early diagenetic zone. With continuing diagenesis and increasing depth, smectite changes into an illite/smectite mixed-layer phase and then subsequently into authigenic illite (Hower et al., 1976; Meunier, 2005). The cations released during the illitization of smectite are considered to be sources for a variety of late diagenetic mineral cements. Illitization is typically presumed to provide Fe and Mg for chlorite formation and for ferroan dolomite precipitation (Hower et al., 1976). Illitization is considered a source for Si (Hower et al., 1976; Thyberg and Jahren, 2011) which facilitates quartz cementation.

In the present study we take a closer look at clay diagenetic processes specific to the matrix component of mudstones. We approached this issue by separating matrix clay minerals from the whole mudstone and then analyzing them in detail. This procedure provides detail information about the illitization process and the depth-range over which expandable clay minerals like smectite occur. These insights are not only of scientific interest but are also of importance for the exploration and production of conventional and unconventional hydrocarbon resources. Over the two past decades, shales as reservoir rocks have become of great economic importance. Exploration and production of shale gas and

* Corresponding author.
E-mail address: susanne.gier@univie.ac.at (S. Gier).

https://doi.org/10.1016/j.marpetgeo.2021.105082
Received 14 September 2020; Received in revised form 9 April 2021; Accepted 11 April 2021
Available online 17 April 2021

shale oil is pursued in numerous sedimentary basins around the world, with the most extensive activity located in the continental United States. Hydraulic fracturing is commonly used to facilitate hydrocarbon extraction from fine-grained and low-permeability shale reservoirs. Fluid (water) and proppant (sand) injection (via perforated wellbores) into shale successions increases permeability in the near-well-bore zone and allows contained gases and fluids to be released and produced. Both the brittleness of the rock and the composition of the matrix, especially the content in expandable clay minerals, are important parameters for hydraulic fracturing (Jarvie et al., 2007).

In the present study, we characterize the mineralogy, petrology and diagenesis of the mudstones of the Malmian Mikulov Formation with special emphasis on matrix and pore development. The Mikulov mudstones are the main source rock for oil and gas in the Vienna Basin and reach a thickness of more than 1000 m. In an effort to characterize the potential for shale gas extraction from the Mikulov Formation in the northern Vienna Basin, OMV Exploration & Production commissioned this study on mineralogy and content of expandable clay minerals of the marlstones. 46 core samples from 10 different wells which penetrated the Mikulov Formation over a depth range of 1400 m–8551 m were available. This has provided a unique opportunity to study diagenetic transformations within a single shale package over a wide depth range.

Main research questions addressed are: 1) Can the diagenesis of the clay minerals in the matrix be related to various cements of the Mikulov Formation mudstones? 2) Is there a connection between mineral and organic diagenesis? 3) From a purely mineralogical aspect, do the mudstones hold a shale gas potential?

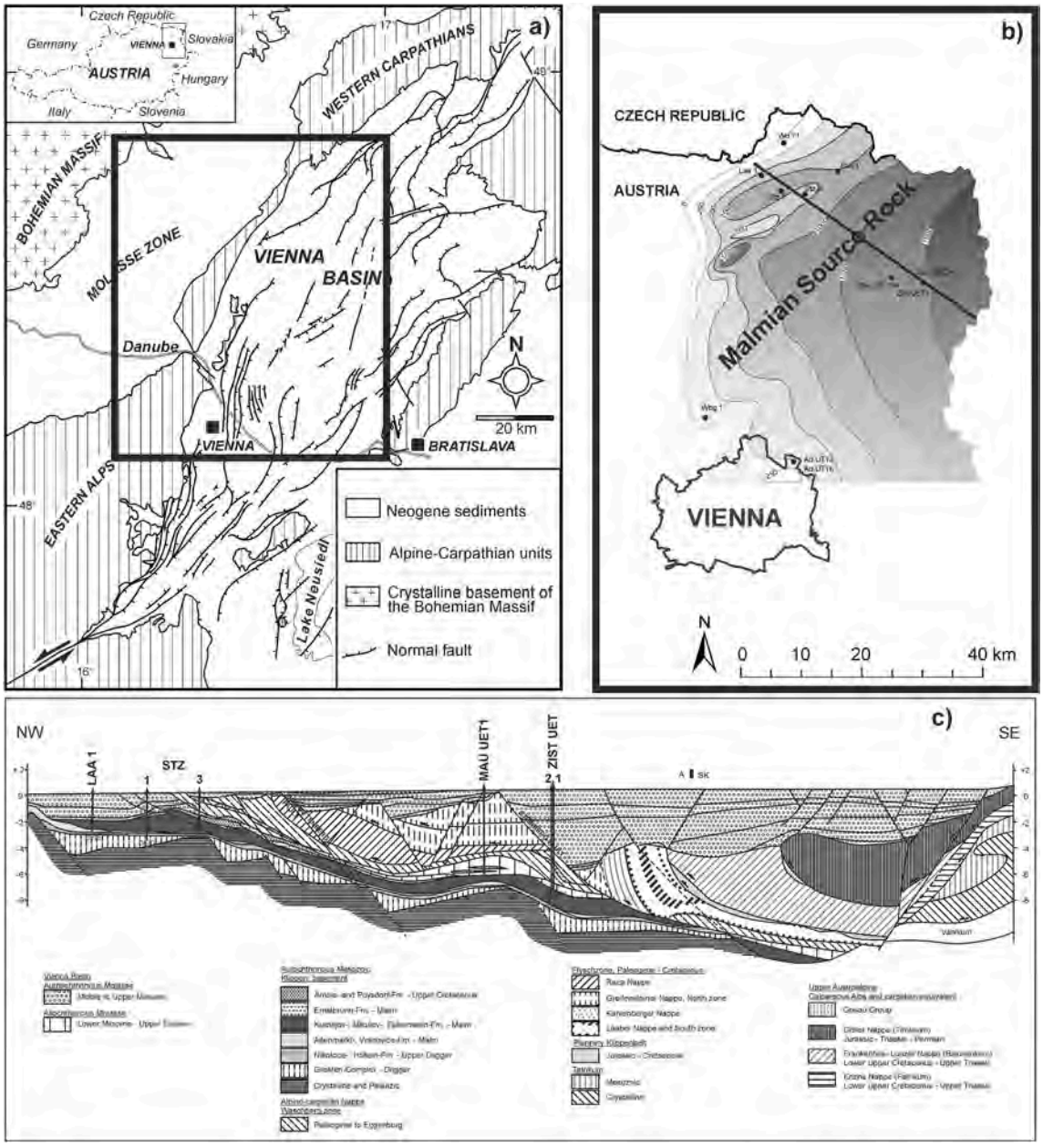

Fig. 1. a) Location map of the Vienna Basin and surrounding areas (adapted from Wagreich and Schmid 2002). Inset shows the location of Fig. 1b. b) Thickness map of the Mikulov Formation in the Austrian part of the Vienna Basin (after Seifert (1996) and OMV internal data) with location of sampled wells. Line indicates cross section shown in Fig. 1c. c) Regional geological cross section through the Vienna Basin and its pre-Neogene floor (modified after Wessely, 2006). Sampled wells (see Table 1) along the section are highlighted.

2. Geology

The Vienna Basin is located in the northeastern part of Austria and extends into Slovakia and the Czech Republic. It trends northeast-southwest, has a rhomboidal shape, and is approximately 200 km long and 40 km wide (Fig. 1a and b). It is a classic pull-apart basin that formed along a sinistral fault system during the lateral extrusion of the Eastern Alps (Royden 1985). Neogene sediment thickness reaches up to 5.5 km in the depocentres. A number of tectonostratigraphic units are distinguished in the Vienna Basin. From bottom to top these are the basement, autochthonous Mesozoic and Permo-Carboniferous sediments, Cenozoic foreland basin sediments, tectonically stacked nappes of the Alpine–Carpathian fold and thrust belt and sediments of the Neogene basin fill (Fig. 1c). During the first phase of its evolution in the early Miocene, the Vienna Basin formed as a piggy-back basin on top of the thrusted and imbricated nappes of the Alpine–Carpathian fold and thrust belt. The second phase of basin formation, the classic pull-apart phase, started in the middle Miocene and continued until the late Miocene, when east–west compression led to basin inversion (Decker and Peresson 1996). From the Pleistocene to present times the basin is characterized by east–west extension.

Permo-Mesozoic sediments of the Northern Calcareous Alps and the Flysch and early Neogene to Paleogene sediments with tectonic imbricates of Upper Jurassic and Cretaceous rocks in the Waschberg Zone make up the nappes underlying the Neogene basin and the Alpine foreland. The nappes of the Alpine–Carpathian fold and thrust belt were thrusted over Cenozoic foreland basin deposits, bracketing the age of thrusting from late Eocene to early Miocene. The Cenozoic foreland basin deposits in turn transgressed over autochthonous Mesozoic sediments of the Lower Austrian Mesozoic Basin (sensu Granado et al., 2017). Locally, Permo-Carboniferous sediments belonging to the Variscan cycle are the oldest sediments (Kroner et al., 2008). The overall thickness of sediments can reach up to 10,000 m (Milan and Sauer, 1996). The Vienna Basin is a major hydrocarbon province and extensive geological research has been carried out for more than 150 years (Sauer et al., 1992). Oil and gas exploration activities started in the early 20th century and first hydrocarbon discoveries were made in the early 1930s. Since then, more than 6000 wells have been drilled (Arzmüller et al., 2006). Most of the oil and gas production comes from Neogene sediments at depths from 1000 to 2000 m. In addition, commercial oil and mainly gas production has also been achieved from within the Alpine - Carpathian fold and thrust belt, with production reaching as deep as 6000 m (Kröll and Wessely, 1973). High oil prices in the 1970s and 1980s put the deep autochthonous Mesozoic sediments below the Alpine - Carpathian fold and thrust belt into the focus of exploration drilling activities. The deepest well, Zistersdorf UET 2A, reached a total depth of 8553 m in basinal mudstones of the Malmian Mikulov Formation (Fig. 1b and c). Based on results of this drilling campaign, several authors have suggested the potential for unconventional gas in the Mikulov Formation (Eliáš and Wessely, 1990; Milan and Sauer, 1996). They proposed that, due to their significant thickness of more than 1000 m, the mudstones of the Mikulov Formation could reservoir large quantities of gaseous hydrocarbons.

The crystalline basement with a local Permo-Carboniferous sediment cover forms an extension of the Bohemian Massif and can be traced some 50 km into the subsurface. The evolution of the Lower Austrian Mesozoic Basin, which represents the Middle Jurassic to Early Cretaceous rifted margin of the European plate can be linked to the development of the Alpine Tethys (eg Wessely 1987; Zimmer and Wessely, 1996; Schmid et al., 2004). Three megasequences, pre-rift, syn-rift and post-rift characterize the passive margin sedimentary fill of the Lower Austrian Mesozoic Basin.

Initial rifting created –northeast to southwest trending half-grabens, which were filled by clastic sediments. Post-rift sedimentation starts with sandy and cherty dolostones. A marine carbonate depositional system was established for the remainder of the Jurassic. Its lowermost units are characterized by clean limestones and dolostones. The Oxfordian to Tithonian Klentnitz Group represents a carbonate ramp to basin system (Fig. 2). The shallow water part in the western part of the basin is represented by the Altenmarkt Formation, the slope by the Falkenstein Formation and the basinal part by mudstones of the Mikulov Formation. The spatial relationship between these three, time equivalent formations

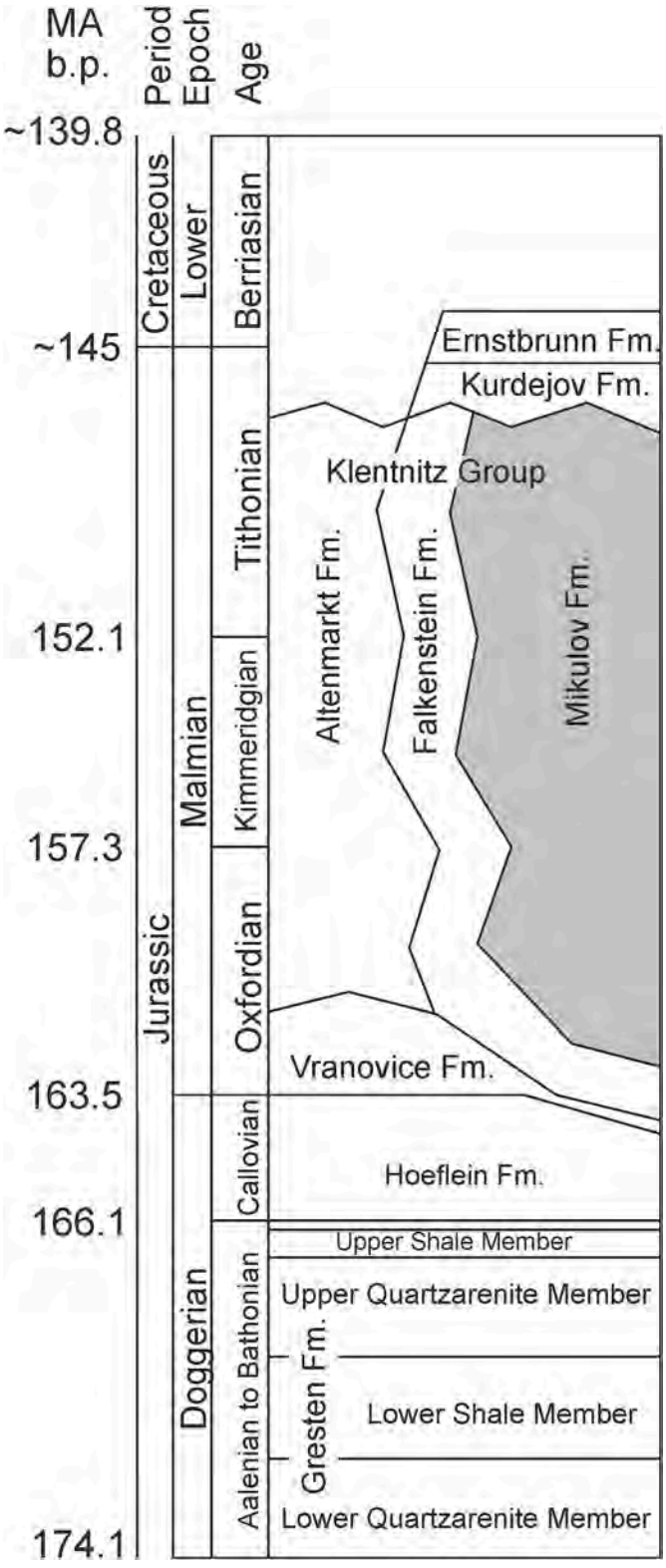

Fig. 2. Jurassic stratigraphy of the Lower Austrian Mesozoic Basin (redrawn from Eliáš and Wessely, 1990 and Rupprecht et al., 2017).

is documented in a number of wells (Wessely, 2006). The transition between the Falkenstein Formation and the Mikulov Formation is characterized by a grain size decrease and the onset of turbiditic sediments (Rupprecht et al., 2017). Regionally, going more basinward to the east, the Mikulov Formation becomes more distal and thickens (Fig. 1b). While tectonic thickening cannot be completely ruled out, recent microfacies and biomarker work by Rupprecht et al. (2017) points to the thickness being of primary sedimentary origin. There are also indications that the original TOC content increased in a basinward direction (Rupprecht et al., 2017). The youngest part of this carbonate sequence are shallow water limestones of Tithonian to Berriasian age. A period of regional uplift and erosion followed. The youngest sediments of the Lower Austrian Mesozoic Basin are locally-preserved sands, shales and marls of a Late Cretaceous age.

Mudstones of the Malmian Mikulov Formation are the main source rock in the Vienna Basin, which has a present day geothermal gradient of 22–26 °C/km (Milan and Sauer, 1996; Sachsenhofer, 2001). Peak oil maturity (~0.85% Rr) is reached at a depth of around 4500 m (Rupprecht et al., 2017). Triggered by thrusting, the Mikulov Formation entered the oil window in the Early Miocene (Ladwein, 1988). Local Neogene subsidence controlled its further maturation. Depending on location, the present-day maturity ranges from being in the oil window to overmature. The present-day depth of oil generation is between 4000 and 6000 m (Ladwein, 1988).

3. Materials and methods

3.1. Materials

Forty-six samples from cores of 10 wells were provided by OMV covering the Mikulov Formation in the northern part of the Vienna Basin, the Waschberg Zone and the Alpine Foreland (Fig. 1a-c, Table 1). The shallower samples are brittle, massive and grey. Some samples show lamination and others contain bright calcite veinlets in an angle to the bedding. The deeper samples are black to dark grey in colour, massive, fine grained and some show slickensides.

3.2. Methods

In a first step for the sample preparation, the core samples were washed with water. Then the outermost centimeter of the core was removed to avoid possible contamination from drilling fluids.

Table 1
Sample list with depths and wells (Ad-Aderklaa, Falk-Falkenstein, Mau-Maustrenk, Stz-Staatz, Wbg-Waschberg, Wd-Wildendürnbach, Zist-Zistersdorf) and bulk mineralogy from XRD in vol % (clay min-clay minerals, ank-ankerite, sid-siderite, arag-aragonite, plag-plagioclase). TOC-values in wt %.

well	sample (m)	quartz	clay min	calcite	ank	sid	arag	plag	pyrite	TOC
Wd T1	**1449.1**	10.8	33.4	51	1.6			1.5	1.7	1.87
Stz 1	**2084.1**	16.6	36.6	42.6	1.6			1.4	1.1	1.20
Stz 1	**2143**	16.9	31.7	47	1.3			1.2	2	0.93
Stz 1	**2178**	14.1	23.7	57.5	2.3			1	1.4	1.82
Stz 1	**2213.5**	14	33.5	47.7	1.5			2.3	1	1.15
Stz 1	**2283.93**	21.7	33	35.5	5.8			2.9	1.1	1.23
Stz 1	**2324.3**	10.8	28.9	57.1	1.1			1	1	1.38
Laa 1	**2325.7**	10.4	28.1	56.9	2.3			1.2	1	0.98
Stz 1	**2358.65**	13.4	26.1	55.2	2.8			1	1.5	1.16
Stz 1	**2414.95**	15.2	28.5	52.13	1.9			1.4	0.9	1.37
Stz 1	**2466.95**	14.7	26	51.6	5			1	1.7	1.24
Stz 3	**2476.3**	12.2	23.1	59	5.1				0.6	0.92
Stz 3	**2479.8**	11	18.5	69.3	0.8				0.4	0.88
Laa 1	**2491**	11.3	18.2	68	2.2				0.4	0.82
Stz 1	**2521.92**	14.6	31.4	48.4	1.15		1.15	1.05	2.25	1.81
Wbg 1	**2537.55**	10.8	28.5	57.1	2.2				1.4	1.51
Laa 1	**2557.3**	10.1	16.2	70.4	2.2				1.2	0.86
Stz 1	**2578**	12	28.4	57.6	1.4				0.6	1.02
Stz 1	**2631**	13.9	21.2	59.5	3.1			1.4	0.9	1.7
Laa 1	**2663.1**	4.8	13.8	77.5	2.7				1.2	0.76
Stz 1	**2687**	13.1	30.3	52.7	2			1	0.8	1.58
Stz 1	**2741**	10.5	22.6	63.2	2.3			1	0.5	1.27
Laa 1	**2748.1**	8.6	21.9	62.5	4.8			1.3	1	0.69
Stz 1	**2774.5**	9.2	26.6	60.5	2.3				1.4	1.42
Stz 1	**2824**	10	23.8	63.6	0.9			1.1	0.6	1.09
Laa 1	**2833**	8.1	29.7	51.4	8.7			1.4	0.6	0.55
Laa 1	**2895**	8.1	19.7	70.5				1.2	0.7	0.77
Stz 1	**2940.5**	2.6	15.2	80.2	1.4				0.5	0.6
Stz 1	**2996.7**	9.8	29.7	56.3	2.1			1.4	0.6	1.00
Stz 1	**3097**	9.2	26	56	7.8				1	0.37
Falk 1	**3746.1**	12.8	27.6	54.4	3			1.2	1.1	1.55
Falk 1	**3956.9**	12.6	25.8	61				0.6		1.67
Falk 1	**4151.65**	20.6	46.9	20.1		1.8		3.8	6.8	1.28
Zist UET2A	**5586**	8.8	38.7	41.5	1.5		3.7	1.7	4	3.09
Zist UET1	**5604.3**	19	42.8	32.9		1.3		2.4	1.7	2.58
Zist UET1	**5672.7**	17.1	39.1	36	1.8	1.8		2.3	1.9	2.79
Zist UET1	**5738**	14.4	34.4	39.6	9.3			1.3	1.1	1.83
Zist UET1	**5979.5**	17.4	36.6	37.1	4.6			2.8	1.6	2.25
Ad UT 1a	**6079.9**	15.7	30.2	45.5	5.3			2.3	1	0.85
Ad UT 1b	**6220.8**	13	35.1	44.7	3.7			2.5	1	1.38
Mau UET1a	**6551.5**	16.8	32.7	44.3	2.8			2.2	1.1	1.18
Zist UET2A	**7704.7**	17	40	36.1	2.7			2.6	1.6	1.84
Zist UET2A	**8159.7**	9.6	30.2	57.3	1.5			1	0.5	0.56
Zist UET2A	**8546.7**	12.5	29.1	54.5	1.8			1.5	0.7	0.67
Zist UET2A	**8549.4**	15.7	26	53.1	1.6			1.5	2.1	1.28
Zist UET2A	**8551.7**	11.1	14.4	71.4	1.2			1.3	0.6	0.57

3.2.1. Thin section microscopy

Thin sections of the samples were provided by OMV and were examined with a Leica DM 4500P optical microscope, equipped with a digital colour camera.

3.2.2. X-ray diffraction (XRD)

3.2.2.1. Sample preparation. For the analysis of the bulk mineralogy with X-ray diffraction, powdered samples were prepared with an agate mill. The samples were prepared non-oriented with sand-paper and additionally oriented by saturating the sample with ethylene-glycol for semi-quantitative analysis after Schultz (1964).

For separation of the <2 μm fraction, parts of the core samples were carefully crushed to a grain size of approximately 2–3 mm. The crushed samples were then treated with 0.1 *M* EDTA solution (pH 4.5) at 50 °C to dissolve and remove the carbonates and free iron oxides (Glover, 1961). EDTA was removed by centrifugation and subsequent washing with water. Further disaggregation was achieved with a 400 W ultrasonic probe for 3 min. The <2 μm fraction was separated by sedimentation in an Atterberg cylinder (DIN 51033, 1962) and dried at 50 °C. The homogenised samples were saturated with K^+ and Mg^{2+} ions and oriented samples were prepared by dispersing 8 mg of clay in 1 ml of water and pipetting the suspensions onto glass slides. The oriented, K- and Mg saturated samples were analyzed in air-dried state and after saturation with either ethylene glycol or glycerol at 60 °C for 24 h to identify expandable clay minerals like smectite. Additionally, K-saturated samples were heated to 550 °C C to destroy kaolinite and expandable clay minerals (Moore and Reynolds, 1997).

The <0.2 μm fraction was separated by centrifugation of the <2 μm fraction for 21 min at 4500 rpm according to Tanner and Jackson (1948). The resulting suspensions were concentrated by evaporation and freeze-dried with an Alpha 1–4 LSC-Christ freeze drier (0.5 mbar vacuum). Approximately 20 mg of the <0.2 μm fraction was dispersed in 1 mg distilled water and sedimented on glass slides and analyzed air dried and saturated with ethylene glycol.

Oriented <2 μm fractions of the samples and four standards (SW1, SW2, SW4 and SW6; Warr and Rice, 1994) for illite crystallinity (IC) determination were prepared on glass slides (8 mg/ml). The standards of Warr and Rice (1994) origin from the Variscan very low-grade metamorphic belt in north Cornwall, SW England and represent an increasing metamorphic grade. Standard SW1 is a silty mudstone that underwent late diagenetic alteration, whilst the silty mudstone SW2 lies at the anchizonal boundary. Standard SW4 is a grey slate from within an area of anchizone alteration and standard SW6 is a grey-green slate from the epizone (lower greenschist facies). The values of the Crystallinity Index Standard (CIS) scale decrease with increasing metamorphic grade: (001) IC values for SW1, 2, 4 and 6 are 0.63, 0.47, 0.38° and 0.25°Δ2θ, respectively.

3.2.2.2. Data processing. Semi-quantitative mineral estimates of the bulk sample were done using the method of Schultz (1964) which has error limits of ±10%. The clay mineralogy was quantified by using two methods to achieve more accurate results: the mineral intensity factors (MIF) by Moore and Reynolds (1997) and a modified version of Schultz (1964). For the latter method, the correction factors were adapted to quantify the <2 μm fraction. The proportions of smectite and illite in the I-S phase were determined using the 2-theta method described by Moore and Reynolds (1997).

For illite crystallinity (IC) determination, the half-peak-width of the 10 Å illite peaks of the <2 μm fractions and the standards (Warr and Rice, 1994) were measured. Calibration of the raw (001) IC-values was undertaken with the following regression equation, determined from plotting the measured (001) IC peak-widths against the quoted values in Warr and Rice (1994):

$IC_{calibrated} = 1.3648 * IC_{measured} + 0.0677$, with a correlation coefficient (R^2) of 0.980.

3.2.2.3. Analysis. The bulk mineralogy and the <2 μm fraction were analyzed with a PHILIPS PW 3710 X-ray diffractometer (CuKα radiation, 45 kV, 35 mA, step scan, step size 0.02, 1s per step). The <0.2 μm fraction and the <2 μm fraction for illite crystallinity determination were measured with a Panalytical PW 3040/60 X'Pert PRO X-ray diffractometer (CuKα radiation, 40 kV, 40 mA, step size 0.02, 5s per step).

3.2.3. Chemistry of the fine clay fraction

The <0.2 μm fractions of three samples from different depths (2833 m, 5604 m and 7704.7 m) were solubilized with HF/HNO_3 and NaOH (Hu and Qi, 2014). For the HF/HNO_3 dissolved samples, a 100 mg sample mixed with HF and 6 N HNO_3 was placed on a water bath. The samples were 'washed' five times with the acids and then filled up with 100 ml H_2O_{dest} in flasks. For the NaOH dissolved samples, 250 mg sample and 1.5 g NaOH were slowly dissolved and filled with H_2O_{dest} up to 250 ml. The major elements were measured by a PerkinElmer ICP-OES, Optima 5300 DV. The loss of ignition was measured with a LECO RC-612 Carbon Analyzer (LECO Instruments GmbH) using 100 mg sample.

3.2.4. Total organic carbon (TOC)

100 mg of the powdered samples was measured with a LECO C200 Carbon Analyzer. To determine the TOC, the samples were heated up to 550 °C and to determine the TC (total carbon) they were heated up to 1000 °C.

3.2.5. Scanning electron microscope (SEM)

SEM analysis was undertaken on broken surfaces and on argon ion milled surfaces. For information on crystal morphologies of the diagenetic minerals, split samples were coated with gold and examined with a PHILIPS-XL 30 ESEM equipped with an energy-dispersive spectrometer at the University of Vienna.

For pore-type analyses and petrology, thin slices of the samples were mounted on a sample holder and polished via edge milling with a GATAN Ilion argon-ion mill. The samples were not cooled during the milling process. Milled surfaces were then examined by SEM without conductive coating (FEI Quanta 400 FEG, low-vacuum mode) at Indiana University. All samples were viewed on surfaces oriented perpendicular to bedding.

4. Results

Thin section analysis together with XRD results were used for the classification of the rocks and the nomenclature of Lazar et al. (2015) was applied. Samples with more than 50% carbonate and more than 50% grains coarser than 63 μm were classified after Dunham (1962).

4.1. Thin section microscopy

Sample 2479.8 m (Fig. 3a) is a coarse-grained, poorly sorted packstone (Dunham (1962). The sample contains monocrystalline quartz, calcite, glauconite, mica, dissolved radiolarians filled with calcite and pyrite. Benthic foraminifera and sponge needles are common. Well rounded as well as angular components are present. Moulds from dissolved fossils are filled with calcite or calcitic overgrowth.

Sample 2557.3 m (Fig. 3b) is a coarse-grained, poorly sorted wackestone (Dunham, 1962). The sample contains foraminifera, dissolved radiolarians filled with calcite, and rounded micritic clasts. The sample contains a large amount of sponge needles and mollusc shells filled with microcrystalline calcite.

Sample 5738.0 m (Fig. 3c) is a calcareous-argillaceous mudstone (Lazar et al., 2015) and contains quartz, glauconite and sponge needles

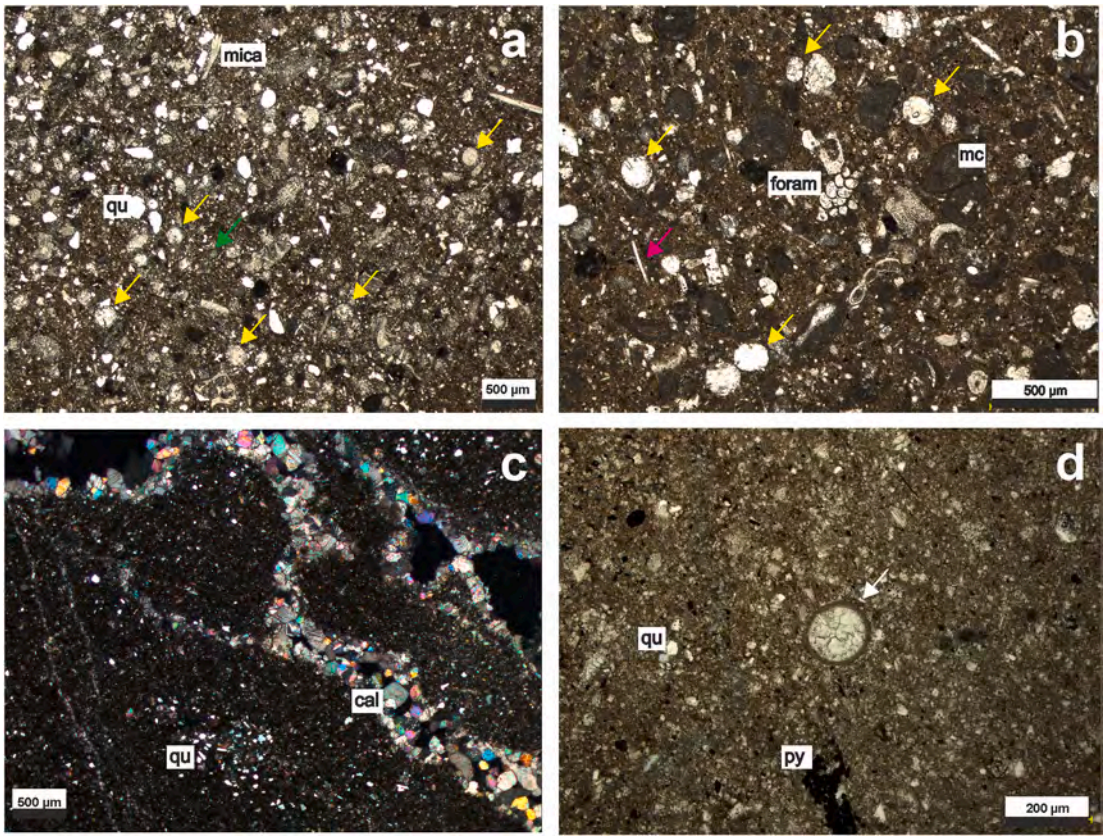

Fig. 3. Thin section photomicrographs of a) sample 2479.75 m, plane-polarized light (PPL): Poorly sorted packstone with monocrystalline quartz (qu), calcite, glauconite (green arrow), mica, dissolved radiolarians filled with calcite (yellow arrows), and pyrite. Benthic foraminifera and sponge needles are common; b) sample 2557.3 m (PPL): Poorly sorted wackestone (Dunham, 1962), containing foraminifera (foram), dissolved radiolarians filled with calcite (yellow arrows), rounded micritic clasts (mc), large amounts of sponge needles (pink arrow) and mollusc shells; c) Sample 5738.3 m, cross-polarized light (XPL): Calcareous-argillaceous mudstone (Lazar et al., 2015) with quartz (qu), glauconite and sponge needles filled with sparite. Microfractures dissect the sample, they are either fully filled with calcite (cal) or partially open and lined with calcite; d) Sample 6220.85 m (PPL): Moderately sorted, coarse-grained calcareous-argillaceous mudstone (Lazar et al., 2015) with scattered quartz (qu) grains and disseminated to patchy pyrite (py). A sparite-filled sphere (arrow) is located in the center of the picture. (For interpretation of the references to colour in this figure legend, the reader is referred to the Web version of this article.)

filled with sparite. Microfractures dissect the sample, they are either fully filled with calcite or partially open and lined with calcite.

Sample 6220.8 m (Fig. 3d) is a moderately sorted, coarse-grained calcareous-argillaceous mudstone (Lazar et al., 2015) with scattered quartz grains and disseminated to patchy pyrite. A sparite-filled sphere is located in the center of the picture.

4.2. Bulk mineralogy from XRD and thin sections

The main components of all samples are calcite, clay minerals and quartz (Table 1, Fig. 4). The bulk samples also contain 1-9 vol% ankerite/dolomite, 1–7 vol% pyrite and 1–4 vol% plagioclase. The most abundant mineral is calcite with 20–80 vol% followed by bulk clay minerals with 14–46 vol% and quartz with 2–21 vol%. The calcite content is made up by biogenic calcite clasts (e.g. foraminifera and shell fragments in Fig. 3 a,b), some detrital calcite grains and calcite cement (Figs. 3c and 9 b, c and Fig. 10 l, m). Bioclasts have been recrystallized into microcrystalline calcite and sparite.

According to the bulk XRD mineralogy and applying the nomenclature of Lazar et al. (2015) two different types of mudstones can be distinguished; calcareous-argillaceous mudstones with a carbonate content of 25–50 vol% and calcareous mudstones with 50–82 vol% carbonate.

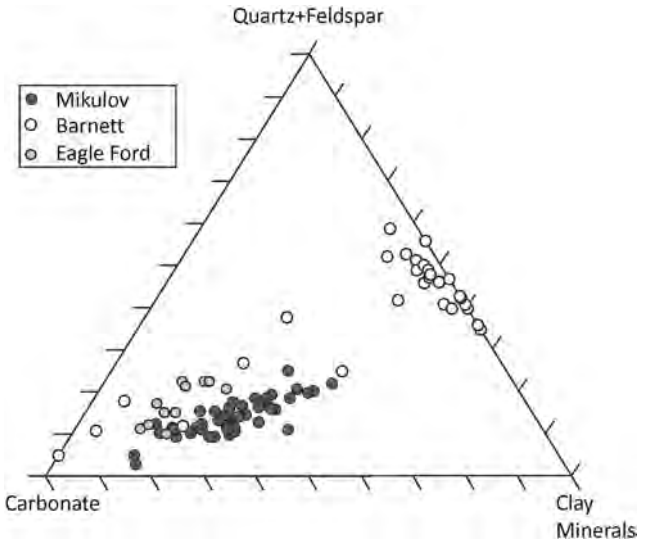

Fig. 4. Distribution of quartz (+feldspar), carbonate and clay minerals from XRD data in the Mikulov Formation. Data from Barnett shale (Jarvie et al., 2007) and Eagle Ford shale (Asala et al., 2016) for comparison.

4.3. Clay mineralogy from XRD

The most abundant minerals in the <2 μm fraction are mixed-layer illite-smectite (I–S) and illite (Table 2). In addition, the clay fraction contains chlorite and kaolinite (Figs. 5 and 6; Table 2). The amount of I–S (68.5–7.6%) and kaolinite (8.1–0%) decreases with depth, whereas both the illite (23.2–70%) and chlorite (0.3–22.4%) contents increase with depth (Figs. 5 and 6).

Illitization of smectite takes place with increasing depth of burial. The X-ray patterns show that the illite content of the mixed-layer clay mineral increases with depth. The shallow samples contain up to 75% smectite in the mixed-layer, an amount that decreases to 10% or less smectite in the deepest samples. In parallel, the ordering (Reichweite, R) of the mixed-layer changes from random interstratification (R0) to ordered interstratification (R1 and R3; Fig. 5e); Moore and Reynolds (1997). This is presented in Fig. 6 where the shallowest sample, at 1449 m, contains a randomly interstratified I–S mixed layer (R0) with a prominent peak at 5.2 °2θ (17 Å) and a 002/003 reflection at 16.0 °2θ; the mixed layer contains 25% illite. The I–S in sample 3956 m is R1 ordered, indicated by a reflection near 6.5 °2θ (13.3 Å); 75% illite in I–S. R3 ordering of the I–S in sample 5738 m is shown by the broad shoulder at 8.2 °2θ (11.1 Å), this sample contains >90% illite in I–S (Fig. 6). The 001/002 reflection of the mixed layer also changes position with depth, it shifts towards the illite 8.8°2θ peak (Fig. 6).

Randomly ordered R0 mixed-layer I–S minerals can be found in samples between 1449 m and 2824 m, and the I–S contains less than 50% illite. The R1 ordered samples from 2833 m to 3956 m contain between 70 and 80% illite. The deeper samples (3097 m–8551 m) contain between 83 and 88% illite and are R3 ordered. The change from random (R0) to ordered (R1) mixed-layering occurs at a depth of about 2800 m at 71% illite in illite/smectite, and corresponds to a temperature of ±93 °C.

The absolute quantity of smectite in the bulk sample was calculated by taking the percentage of smectite in the <2 μm fraction and multiplying it by the percentage of clay in the bulk sample. The absolute quantity of expandable clay minerals decreases with depth. The content of expandable smectite in the bulk samples ranges from 16% in the shallow samples to 0.3% in the deepest sample (Table 2).

4.4. Illite crystallinity

Illite crystallinity (IC) is a parameter that characterizes the degree of very low-grade metamorphism (Warr and Rice, 1994; Merriman and Frey, 1999). Clay-mineral crystallinity reflects a combination of the

Table 2
Relative proportions of illte, chlorite, kaolinite and mixed-layer illite/smectite (I/S) in the clay fraction. The percentage of illite in the mixed-layer illite/smectite (% illite in I/S) and the ordering (R) of the mixed-layer are given as well as the percentage of smectite (% S) in the bulk samples.

well	samples (m)	illite	chlorite	kaolinite	I/S	% illite in I/S	ordering R	% S in bulk samples
Wd T1	**1449.10**	32.1	0.9	0.7	66.3	25.0	0	13.2
Stz 1	**2084.10**	32.2	1.7	3.2	62.8	25.0	0	16.2
Stz 1	**2143.00**	31.9	2.0	4.0	62.0	17.0	0	14.6
Stz 1	**2178.00**	34.3	1.4	2.3	61.9	25.0	0	10.2
Stz 1	**2213.50**	35.3	2.7	4.9	57.0	20.0	0	15.6
Stz 1	**2283.93**	40.8	1.1	2.5	55.6	38.0	0	11.9
Stz 1	**2324.30**	32.7		6.5	60.7	25.0	0	12.9
Laa 1	**2325.70**	34.5	1.8	4.4	59.4	24.0	0	13.3
Stz 1	**2358.65**	53.1	1.7	2.9	42.4	41.0	0	7.8
Stz 1	**2414.95**	41.8		6.7	51.4	20.0	0	11.4
Stz 1	**2466.95**	44.6	2.7	3.6	49.0	38.0	0	8.4
Stz 3	**2476.30**	34.6	0.4	0.5	64.5	29.8	0	9.2
Stz 3	**2479.80**	43.5	0.5	0.4	55.7	34.0	0	8.5
Laa 1	**2491.00**	34.3	1.8	2.3	61.6	38.0	0	6.1
Stz 1	**2521.92**	35.9	1.8	3.3	58.9	39.6	0	9.1
Wbg 1	**2537.55**	37.2	4.1	3.1	55.5	44.0	0	9.3
Laa 1	**2557.30**	36.5	1.9	3.6	57.9	24.5	0	5.6
Stz 1	**2578.00**	38.8	2.8	4.6	53.8	29.8	0	11.6
Stz 1	**2631.00**	31.9	2.2	6.1	59.9	39.5	0	7.2
Laa 1	**2663.10**	39.1	1.1	1.9	57.9	44.5	0	4.7
Stz 1	**2687.00**	37.1	2.7	5.5	54.7	39.6	0	9.9
Stz 1	**2741.00**	32.8	3.4	6.2	57.5	49.8	0	6.5
Laa 1	**2748.10**	45.8	0.3	0.5	53.4	45.0	0	5.5
Stz 1	**2774.50**	33.9	1.6	5.5	58.9	41.0	0	8.6
Stz 1	**2824.00**	44.7	0.4	0.8	54.2	49.8	0	7.1
Laa 1	**2833.00**	44.4	0.7	0.9	54.1	70.2	1	3.7
Laa 1	**2895.00**	31.2		1.2	67.6	58.2	1	5.2
Stz 1	**2940.50**	35.4			64.6	59.0	1	4.3
Stz 1	**2996.70**	36.6	4.0	2.8	56.6	71.1	1	3.8
Stz 1	**3097.00**	40.8			59.2	94.5	3	1.9
Falk 1	**3746.10**	32.2	3.9	6.8	57.1	68.6	1	5.4
Falk 1	**3956.90**	26.5	5.0	7.6	60.9	79.0	1	3.1
Falk 1	**4151.65**	52.0	9.6	8.9	29.5	94.5	3	2.8
Zist UET2A	**5586.00**	36.6	1.7	3.9	57.8	94.5	3	1.8
Zist UET1	**5604.30**	45.7	1.2	3.2	49.0	92.4	3	2.6
Zist UET1	**5672.70**	45.9	2.3	3.8	48.0	96.7	3	2.5
Zist UET1	**5738.00**	43.3	2.3	4.5	41.9	92.4	3	2.6
Zist UET1	**5979.50**	41.3	2.9	3.0	52.8	94.5	3	3.8
Ad UT 1a	**6079.90**	32.5	2.6	1.9	63.0	88.9	3	1.4
Ad UT 1b	**6220.80**	62.6	6.0		31.4	94.5	3	1.8
Mau UET1a	**6551.50**	57.5	3.6	2.8	36.1	92.4	3	2.3
Zist UET2A	**7704.70**	47.1	1.5	1.4	50.0	93.7	3	2.2
Zist UET2A	**8159.70**	64.2	12.7		23.1	95.3	3	1.3
Zist UET2A	**8546.70**	69.9	13.6		16.5	89.0	3	1.0
Zist UET2A	**8549.40**	64.9	14.1		21.0	90.2	3	1.0
Zist UET2A	**8551.70**	70.4	22.6		7.0	88.1	3	0.3

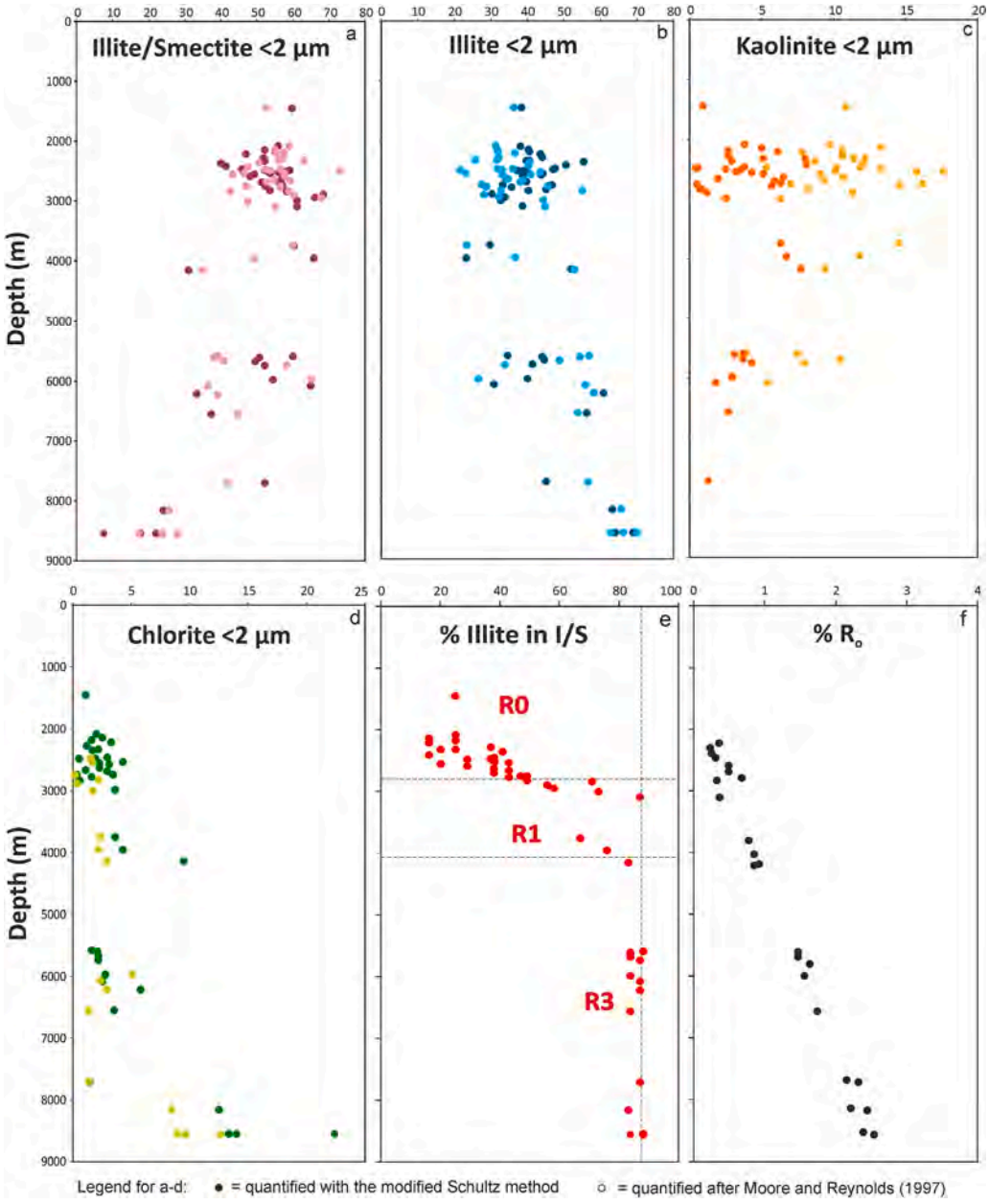

Fig. 5. Changes of the <2 µm fraction with depth (in %) for a) illite/smectite; b) illite; c) kaolinite; d) chlorite. Legend for a–d: dark colors quantified after Schultz (1964) and light colors quantified after Moore and Reynolds (1997); e) % illite in mixed layer illite/smectite; f) vitrinite reflectance (% R_o) with depth after Ladwein (1988) and Rupprecht et al. (2017). (For interpretation of the references to colour in this figure legend, the reader is referred to the Web version of this article.)

thickness of the X-ray scattering domain size (crystallite size) and broadening due to the presence of mixed-layered phases (Merriman and Frey, 1999).

The (001) IC was measured for 12 samples, ranging in depths from 5586 m to 8551.7 m (Fig. 7). The IC of the shallower samples with higher smectite content could not be determined because of peak broadening and overlapping illite/smectite and (likely detrital) illite peaks which makes fitting impossible. The IC °Δ2θ values decrease with depth and increasing temperature from 2.14 to 0.83°Δ2θ hence, the crystallinity increases with depth and temperature (Fig. 7). The CIS scale has anchizonal boundary limits of 0.25°Δ2θ and 0.42°Δ2θ (Warr and Rice, 1994); these are currently thought to approximate to 300 °C and 200 °C (Merriman and Frey, 1999). Compared with the CIS scale of Warr and Rice (1994), the samples are still in the diagenetic zone, even at a depth of 8500 m the samples do not reach the anchizone (Fig. 7).

4.5. Chemistry of the fine clay fraction

The chemistry of the <0.2 µm fraction was analyzed to identify the changes of the chemical composition caused by the diagenetic smectite to illite transformation. The samples were selected according to the ordering of the I–S mixed-layer (R1 and R3). The fine clay fraction was taken, because the coarse clay fraction (<2 µm) not only contains the I–S mixed-layer but also illite, chlorite and kaolinite (Figs. 5 and 6). The calculation of reliable structural formulae requires a purified I–S mixed-layer mineral sample (Köster, 1982). Because of the very small sample quantity available, only three samples could be analyzed chemically (Table 3).

On the basis of 10 oxygens and 2 hydroxyl-groups (which give a total negative charge of 22), the crystal-chemical structural formulae formulae of 2:1-phyllosilicates were calculated (Marshall, 1949; Köster, 1977). The calculations for three selected samples gave the following

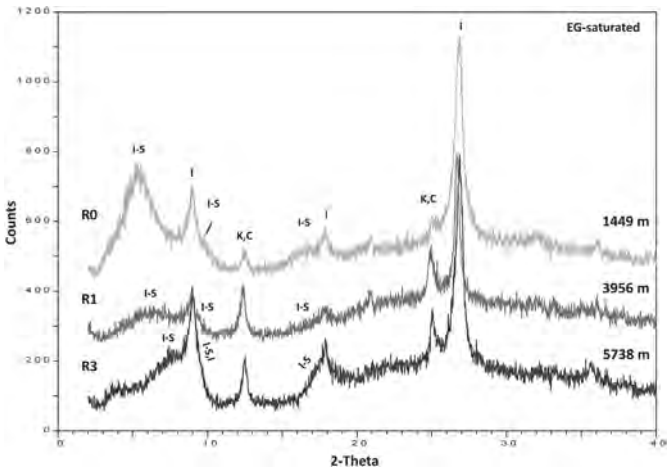

Fig. 6. XRD patterns of ethylene-glycol saturated samples 1449.1 m, 3956.9 m and 5738.0 m; I–S = illite-smectite, I = illite, K = kaolinite, C = chlorite. R = Reichweite.

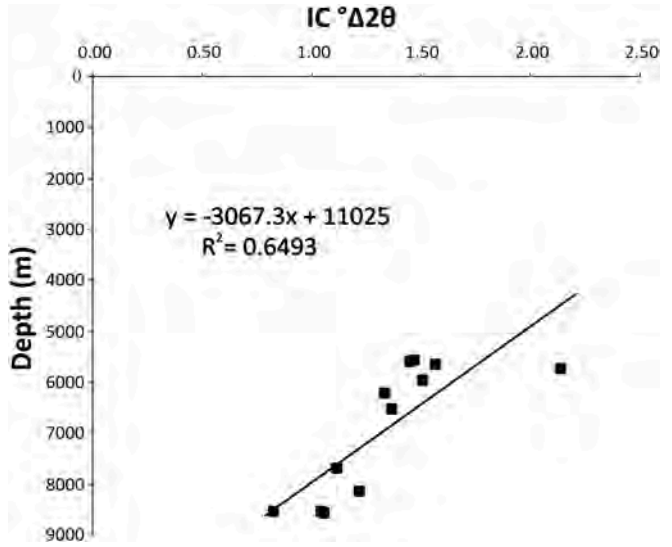

Fig. 7. Illite crystallinity values (°Δ2θ; after Warr and Rice (1994) versus depth (m) for R3 illite/smectite.

results (Table 3):

Sample 2833 m: $(K_{0.33}Na_{0.11}Ca_{0.09})(Al_{1.48}Fe_{0.19}Mg_{0.35}Ti_{0.009}Mn_{0.001})(Si_{3.63}Al_{0.37})O_{10}(OH)_2$

Sample 5604 m: $(K_{0.37}Na_{0.10}Ca_{0.16})(Al_{1.57}Fe_{0.20}Mg_{0.22}Ti_{0.008}Mn_{0.001})(Si_{3.42}Al_{0.58})O_{10}(OH)_2$

Sample 7704 m: $(K_{0.46}Na_{0.15}Ca_{0.11})(Al_{1.66}Fe_{0.15}Mg_{0.20}Ti_{0.006}Mn_{0.002})(Si_{3.36}Al_{0.65})O_{10}(OH)_2$

The distributions of the charges (Table 3) are plotted in the triangular diagram celadonite-muscovite-pyrophyllite (Fig. 8). The shallower sample (2833 m) plots between the montmorillonite (smectite) and the illite field as expected for I–S mixed-layer minerals. The two deeper samples, 5406 m and 7704 m, plot in the illite field, indicating the higher percentage of illite layers in the I–S mixed-layer.

4.6. Total organic carbon (TOC)

TOC was measured for all bulk samples (Table 1); it varies between 0.37 and 3.09 wt% with an average of 1.3 wt% (n = 46). The overall values are in agreement with TOC values in Rupprecht et al. (2017). Samples from the central wells of the basin have slightly higher TOC values, with 1.59 wt% on average, than samples from the wells at the basin margin with 1.13 wt% on average. Higher TOC values in some of the deeper, more basinward and more mature samples could imply an overall eastward increase in TOC (Rupprecht et al., 2017). Their findings are also supported by our data, where deep sample 5586 m shows the highest TOC value. Generally, in the Upper Jurassic Mikulov Formation of the restricted marine basin facies, the TOC ranges between 0.3 and 5 wt% with an average between 1.5 and 2% (Ladwein, 1988).

Table 3
Chemical composition of the <0.2 μm fraction (wt%) and calculated structural formulae (based on O10 (OH)2).

	Laa 1–2833.00	Zist UET1 - 5604.30	Zist UET2A - 7704.70
SiO_2	52.59	51.13	44.14
Al_2O_3	22.71	27.23	25.77
Fe_2O_3	3.74	4.05	2.55
CaO	9.57	6.96	13.64
MgO	3.43	2.16	1.71
Na_2O	0.84	0.79	1.03
K_2O	3.79	4.41	4.74
MnO	0.02	0.01	0.03
TiO_2	0.17	0.16	0.11
P_2O_5	0.45	1.06	0.61
sum	97.3	97.96	94.33
tetrahedral position			
Si	3.63	3.42	3.36
Al	0.37	0.58	0.65
Σ charge	15.63	15.42	15.35
octahedral position			
Al	1.47	1.57	1.66
Fe	0.19	0.2	0.15
Mg	0.35	0.22	0.2
Mn	0.001	0.001	0.002
Ti	0.009	0.008	0.006
Σ charge	5.75	5.78	5.83
interlayer position			
K	0.33	0.37	0.46
Na	0.11	0.1	0.15
Ca	0.09	0.16	0.11
Σ charge	0.62	0.8	0.82

4.7. Mineralogy and morphology from scanning electron microscopy of broken surfaces

In sample from 2497.8 m a mica platelet within a matrix of illite/smectite mixed-layer minerals is seen (Fig. 9a). From XRD analyses this I–S mixed layer material is randomly ordered (R0) and has a smectite content of 63% and an illite content of 37%. Note that the morphology of the clay flakes is still smectitic and most of the edges are wavy (Welton, 1984). At some places small filaments (illite?) have started growth out of the smectite flakes. Fig. 9b shows a calcite cemented area in the same sample. More than 3000 m deeper, in sample 5738 m, the matrix is more illitic (Fig. 9c) and the morphology of the I–S mixed-layer material is fibrous (sample 5979.5 m; Fig. 9d). As calculated from XRD patterns, the mixed layer material is R3 ordered and consists of 13% smectite and 87% illite. In sample 5738 m diagenetic quartz is engulfed by calcite cement (Fig. 9c), stating the calcite cement is a later diagentic feature than the quartz overgrowth.

4.8. Petrology, diagenesis and pore types from scanning electron microscopy of ion milled surfaces

Samples from 3746.1 m to 7704.7 m depth were analyzed for their petrology, diagenetic features and pore development (Fig. 10). Encased within a clayey matrix, silt sized particles of quartz, carbonates and detrital phyllosilicates are the main components (Fig. 10 a,e,g,i,k,o). Most of the quartz and calcite grains have detrital cores and are covered by diagenetic overgrowths (Fig. 10 b,c,e,j,m). Quartz overgrowths form euhedral projections into pore spaces (Fig. 10 b,c,d,j). The overgrowths

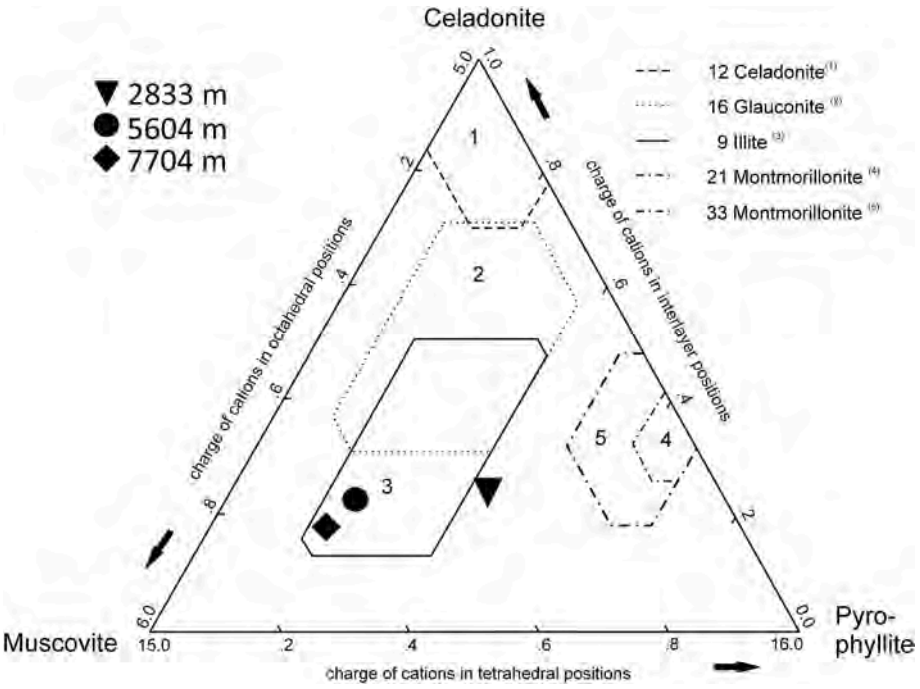

Fig. 8. Triangular diagram for the charge distribution of 2:1 layer silicates with the end-members celadonite-muscovite-pyrophyllite (modified from Köster, 1977).

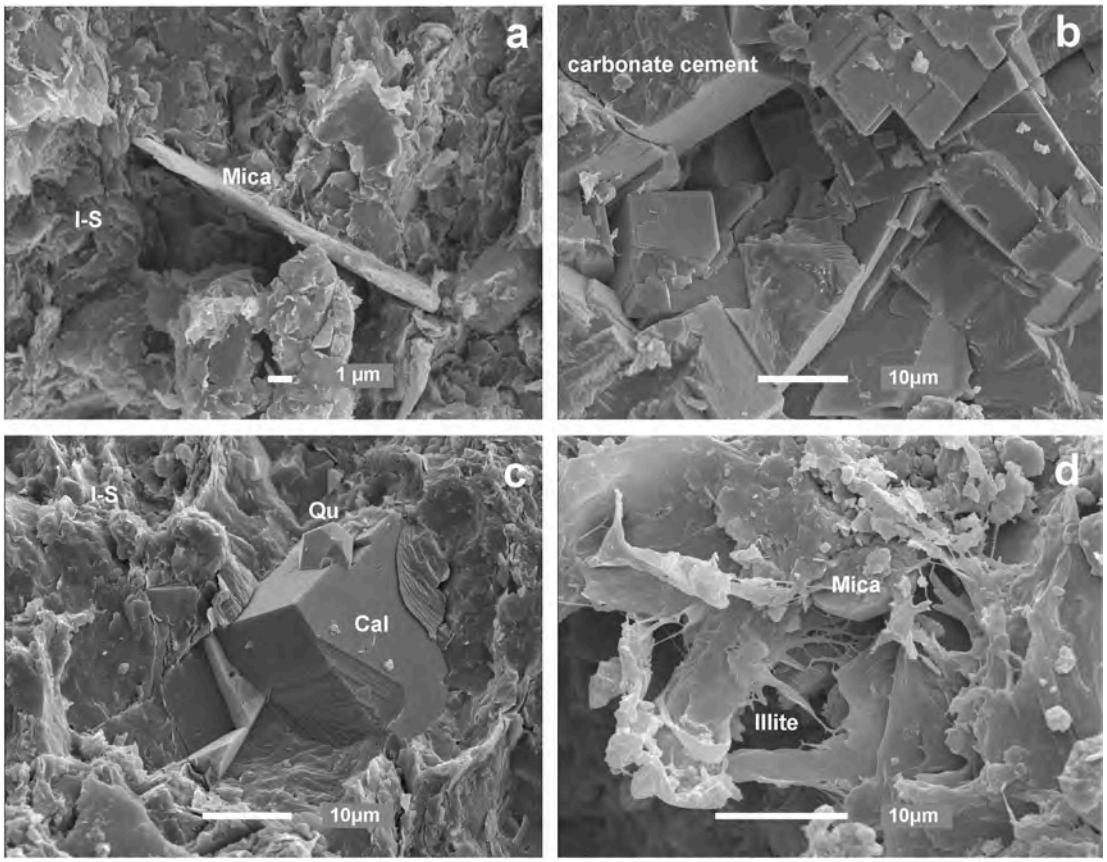

Fig. 9. a) Sample 2497.8 m: Mica platelet within the „matrix", mainly R0 illite-smectite (I-S) mixed layer; b) Sample 2497.8 m: carbonate cement; c) Sample 5738 m: quartz overgrowth (Qu) enclosed by calcite cement (Cal) in a clay matrix; d) Sample 5979.5 m: Illite fibres (R3 illite/smectite) surrounding a mica platelet.

are irregular (Fig. 10e) in the absence of enough pore space. Pyrite is common (Fig. 10 a, g, o) and either forms fine crystalline framboids or occurs as coarser particles several microns in size. Euhedral rhombic carbonate crystals are scattered throughout the samples; they usually have a dolomitic center and iron rich (ankeritic) overgrowths (Fig. 10 a, g,m,o). Organic matter occurs within all samples. Fe-rich phyllosilicates

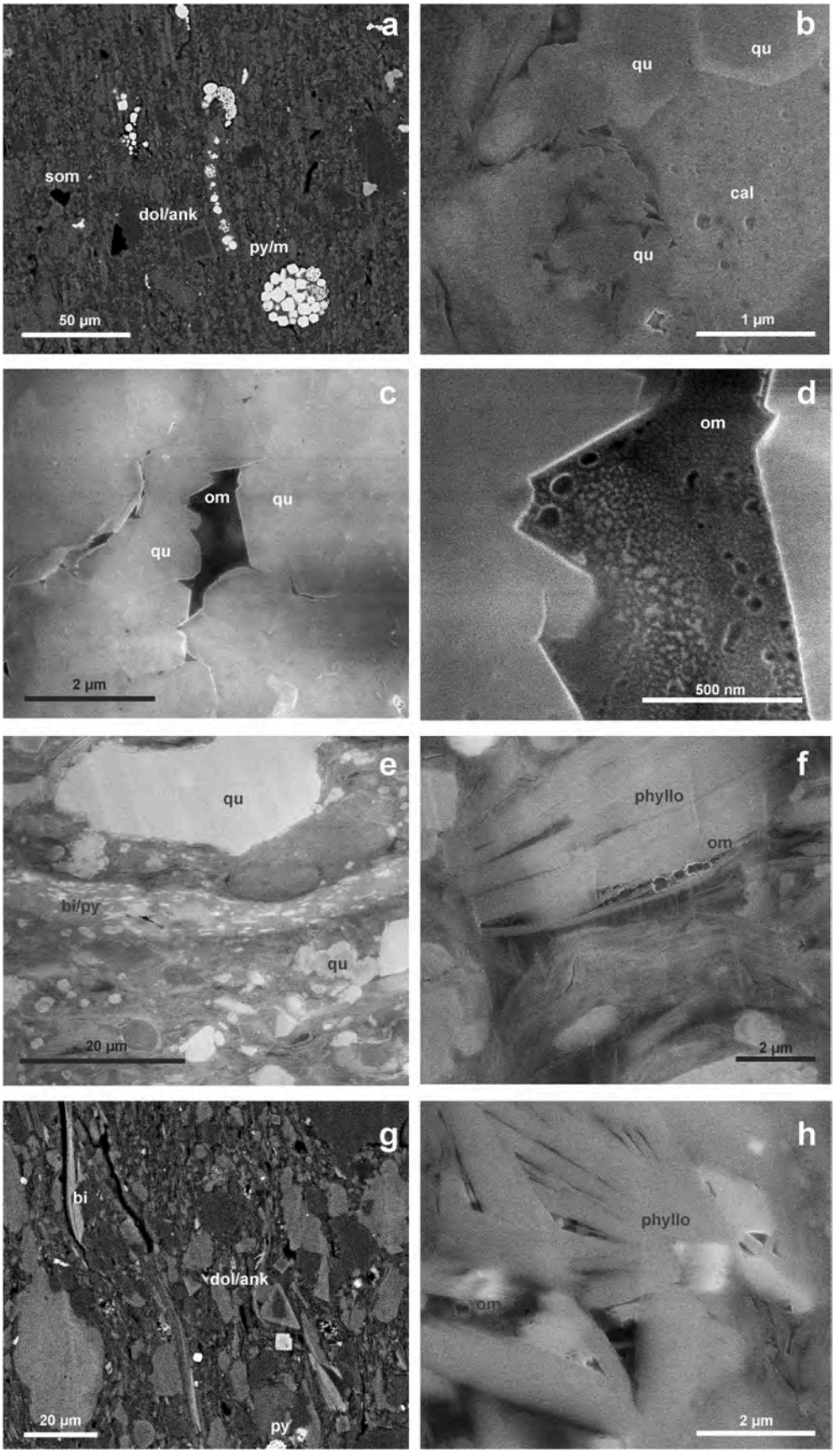

Fig. 10. a) Falk1_3746.1 m: Backscatter image (BSE), showing dense fabric and an abundance of diagenetic iron sulfides (bright). The "string" is a shell fragment that is partially being replaced by pyrite (py)/ marcasite (m). Pyrite forms fine crystalline (0.5 µm) spherical aggregates (framboids), and also occurs as coarser grains several microns in size; possibly marcasite. Dark areas are structured organic matter (som) (Schieber, 2010) without pores. Euhedral rhombic grain in center is dolomite with an iron-rich overgrowth, ankerite (dol/ank); b) Falk1_3746.1 m: Detail view in secondary mode (SE). Quartz overgrowths (qu) on top right side, pores (fluid inclusions) in calcite grain (cal), pores between clamped phyllosilicate and quartz overgrowths; c) Falk1_4151.65 m: SE, euhedral quartz overgrowths enclosing organic matter (om; bitumen) with pores; d) Detail of c) shows blisters on the surface of the organic matter (om) (a beam heating artefact), which suggests that the bitumen still has volatiles that can be mobilized by beam heating (at high magnification); e) Zist UET1_5604.3 m: SE, top: big quartz grain with overgrowths, middle: deformed biotite (bi) with pyrite forming along cleavage planes (Fe derived from alteration of biotite; Schieber, 2011); below right: quartz overgrowths; f) Zist UET1_5604.3 m: SE, organic matter with pores between phyllosilicate (muscovite?) sheets; g) Zist UET1_5979.5 m: BSE, biotite altering to chlorite, structured organic matter, zoned authigenic dolomite-ankerite, pyrite (bright); h) SE, phyllosilicate framework pores filled with organic matter (also containing pores); i) Ad UT1b_6220.8 m: BSE, organic matter with pores between biotite flakes. Biotite flakes clamped in quartz overgrowth. Fabric of calcite grains with clays; clays hindered recrystallization of carbonate mud; j) Ad UT1b_6220.8 m: SE, diagenetic quartz acts as a proppant and keeps pore open; k) MAU UET1a_6551.5 m: SE, quartz with overgrowths, phyllosilicate framework pores (2 µm size), the N–S fracture is artificial; l) MAU UET1a_6551.5 m: Organic matter with pores (both bubble and foam pores); m) MAU UET1a_6551.5 m: Phyllosilicate framework pore, dissolution along dolomite grain margin; n) MAU UET1a_6551.5 m: detail of carbonate dissolution pores; o) Zist UET2A 7704.7: BSE, upper right, biotite/chlorite/kaolinite; middle dolomite rhombs; p) Zist UET2A 7704.7: SE, quartz with overgrowths, organopores, phyllosilicate pores.

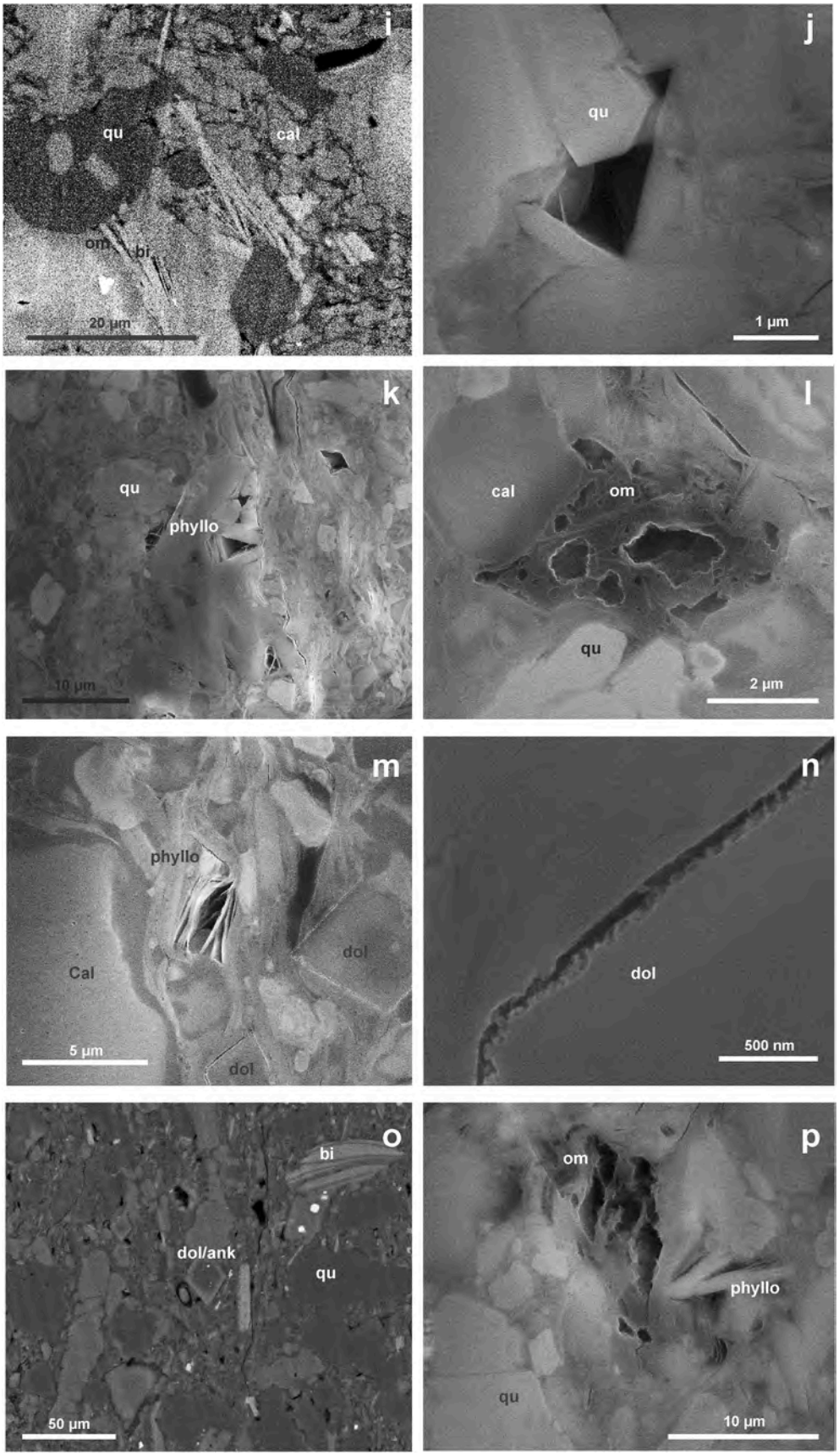

Fig. 10. (*continued*).

identified in BSE analyses, probably biotite or chlorite, are locally altered to non Fe-bearing phyllosilicates, such as kaolinite (Fig. 10 e,g, o). This alteration led to Fe-mineral, such as pyrite, precipitation along cleavage planes (Fig. 10 e; Schieber 2011).

During diagenesis not only cements form, but also μm to nm -size pores are preserved or newly developed because of the properties of initial sediment fabrics, secondary mineral dissolution, and organic matter maturation. Organic matter pores (bubble and foam types) are observed in deeper, thermally mature samples (Fig. 10 c,d,f,h,i,l,p). Phyllosilicate framework pores between phyllosilicate flakes and platelets and associated "hard" grains (Fig. 10 b,h,i,k,m,p) are common. Diagenetic cements, such as quartz overgrowths, newly formed micro-crystalline quartz, as well as carbonate cements have locally prevented pore closure (Fig. 10 b,j,k). Fluid inclusions in calcite and quartz grains can be cut open by the ion beam and manifest as grain-internal pores (intrapores). Partial dissolution of carbonate grains, particularly along grain margins, is a common type of secondary porosity (Fig. 10 b,m,n).

5. Discussion

5.1. Diagenesis of mudstone-matrix and its relation to cementation processes

The illitization of smectite in the matrix can be best traced by using X-ray diffraction analyses of the <2 μm (Fig. 6) and <0.2 μm fractions. The transformation from smectite to illite is one of the best described diagenetic processes throughout global sedimentary basins (e.g. Perry and Hower, 1970; Hower et al., 1976; Franců et al., 1990; Velde and Lanson, 1993; Hillier et al., 1995; Moore and Reynolds, 1997; Gier, 1998; Środoń et al., 2006). In individual basins, the transition from random to ordered interstratification of I-S usually occurs at a range of different depths and temperatures. This is because the illitization process is controlled by several factors, including the primary mineralogical composition of the sediments, time, temperature and especially K^+ availability (McKinley et al., 2003). We compared the illitization process observed in the Mikulov Formation to regionally adjacent Neogene Basins such as the North Alpine Foreland Basin and to other stratigraphic intervals within the Neogene fill of the Vienna Basin. The results are broadly comparable. In the lower Oligocene Schöneck Formation of the North Alpine Foreland Basin, which is the main source rock for oil and gas in this area, ordering occurs at 65% illite in I-S starting at a depth of 3000 m (Gier, 2000). Neogene samples of the Vienna Basin studied by Johns and Kurzweil (1979), Kurzweil and Johns (1981) and Horton et al. (1985) show an ordered phase with 80% illite at 2802 m depth. An exception is the Neogene Pannonian Basin, where the transition takes place at shallower depths starting at 2500 m (Hillier et al., 1995). This can be explained by a slightly higher geothermal gradient of 3.5 °C/100 m when compared to the Vienna Basin. Hower et al. (1976) summarised the following diagenetic mineral reaction for the smectite to illite transformation:

$$smectite + Al^{3+} + K^+ = illite + Si^{4+} \quad (1)$$

But, as Hower et al. (1976) stated, the actual reaction is more complicated, because there is also a release of Fe and Mg from the smectite layers. This Mg and Fe most likely contributes to the formation of chlorite and other Fe-, Mg- containing minerals. From a mineralogical point of view (Hower et al., 1976), the most probable total reaction is:

$$smectite + K - feldspar \ \ (+mica) = illite + quartz + chlorite \quad (2)$$

Kaolinite possibly also takes part in this reaction as it decreases with depth (Hower et al., 1976). In the mudstones of the Mikulov Formation, the content of kaolinite is decreasing with depth, whereas (authigenic) chlorite shows an increase in abundance over the same depth interval (Fig. 5c and d). This distribution pattern could suggest a reaction relationship between kaolinite and chlorite (Boles and Franks, 1979). Because no chlorite/smectite mixed layer minerals were found in the X-ray patterns, chlorite, at least partly, must have had developed from kaolinite.

The reaction would be (Boles and Franks, 1979):

$$3.5\ Fe^{2+} + 3.5\ Mg^{2+} + 9\ H_2O + 3\ \ Al_2\ Si_2\ O_5\ (OH)_4 \ \rightarrow \\ Fe_{3.5}\ Mg_{3.5}\ Al_{6.0}\ O_{20}\ \ (OH)_{16} + 14\ H^+ \quad (3)$$

Calculations of the structural formulae of three illite-smectite mixed layer phases from different depths of the Mikulov Formation show, in accordance to what has been specified by Hower et al. (1976), that K- and Al-ions are needed for the illitization process and that Si, Mg- and Fe-ions are released which could be used for chloritization of kaolinite.

The K- and Al- ions necessary for the transformation from smectite to illite can be supplied from different sources. Dissolution of K-feldspar by acidic pore-waters is a common source (Marfil et al., 2003). Also, decomposition of micas such as muscovite or biotite can act as a supply of K-, Al-, Fe-, Mg- and Si-ions (Boles and Franks, 1979; Van de Kamp, 2016). However, K-feldspar is not present in even the shallowest of the samples from the Mikulov Formation. The absence of K-feldspar is in contrast to the Neogene sediments of the Vienna Basin (Johns and Kurzweil, 1979; Kurzweil and Johns, 1981), and to the sediments of the Pannonian Basin and the North Alpine Foreland Basin (Sachsenhofer et al., 1998; Gier, 2000), where K-feldspar is present. The most likely internal source for K is either muscovite or biotite. In our samples the alteration and splitting open of biotite can be observed with SEM (Fig. 10 e,g,i,o). Commonly a biotite-vermiculite mixed-layer mineral forms as biotite alters (Środoń, 1999). The Fe-ions released during this alteration process favour formation of Fe-minerals (such as pyrite) along cleavage planes (Fig. 10 e). Potassium released from interlayer positions of biotite or muscovite likely contributed to the illitization of smectite. Additionally, the Fe- and Mg-ions released during the illitization of smectite and/or biotite alteration may have supported precipitation of ankerite overgrowths on dolomite (Fig. 10 a,g,m,o). Boles and Franks (1979) suggest that calcite is being converted to ankerite at greater depths (>2500 m), the source of iron and magnesium for this reaction coming from the illitization of smectite:

$$Fe^{2+}Mg^{2+} + 4CaCO_3 \rightarrow 2\ CaFe_{0.5}\ Mg_{0.5}(CO_3)_2 + 2\ Ca^{2+} \quad (4)$$

The main source for diagenetic calcite in the Mikulov Formation is most likely the dissolution of detrital and bioclastic carbonate grains (Fig. 3) and subsequent re-precipitation. According to Hower et al. (1976), authigenic chlorite also forms as Fe and Mg is released during the smectite to illite reaction.

The Si released during the smectite to illite transformation resulted in the precipitation of diagenetic quartz. Additionally, early diagenetic dissolution of radiolaria or other siliceous microfossils could have provided some of the Si for cement formation already early in diagenesis (Schieber et al., 2000). This is supported by the fact that radiolarians and sponge needles replaced by calcite can be observed in almost all thin sections (Fig. 3a and b). Where this quartz precipitates, depends on the geologic context. For example, in the open system reported for the Wilcox Group mudstones (Day-Stirrat et al., 2010), the released Si forms quartz overgrowths in adjacent sandstones, rather than within the mudstones. In closed systems, micro-quartz cements occur within the mudstone matrix as has been described from basins in the Norwegian Sea (Peltonen et al., 2009).

Based on X-ray diffraction data, thin section and SEM analyses, pyrite is present in all Mikulov samples. Pyrite framboids, representing the early stages of sulfate and iron reduction, are typically the earliest precipitates and form close to the sediment-water interface (Morse and Wang, 1997). Multistage early Fe-sulfide diagenesis is suggested by fine crystalline spherical pyrite framboids that follow a shell fragment in Fig. 10a. They are partly replaced by coarser grained marcasite, probably due to re-oxidation of earlier formed framboids (Schieber, 2011).

5.2. Linking inorganic (mineral) to organic diagenesis

Rupprecht et al. (2017) gave a comprehensive summary of the organic geochemistry and maturity of the Mikulov Formation by analyzing 240 source rock samples for TOC, Rock-Eval parameters, vitrinite reflectance, composition of organic matter and hydrocarbons, carbon isotopes of kerogen, and other parameters. Ladwein (1988) described the kerogen type of the Mikulov Formation as II or III. Also Rupprecht et al. (2017) determined Type II kerogen for the Upper Jurassic succession with a relative low HI (<400 mg HC/TOC).

Vitrinite reflectance is a commonly used proxy for source rock thermal maturity. By giving information about burial temperatures it also helps to constrain the diagenetic regime of the inorganic (mineralogical) components of mudstones. Vitrinite reflectance values can be correlated to the illitization of smectite; because both illitization as well as vitrinite reflectance increase with depth (Fig. 5 e,f). In the mudstones of the Mikulov Formation the I-S mixed-layer minerals occur over a reflectance range from 0.49 to 3.34% R_o (Ladwein, 1988) with values of 0.8–1.7% R_o between 4500 m and 6000 m (Ladwein, 1988). The expandability of the mixed layer minerals decreases with increasing vitrinite reflectance and the transition from random to ordered mixed-layering (Fig. 5e) occurs at depth of 2800 m and a vitrinite reflectance of 0.60% R_o (Fig. 5f). This corresponds to reflectance values cited in Kisch (1987) where the transition from random to ordered mixed-layering usually occurs at reflectances of 0.45–0.65% R_o. Generally, the vitrinite reflectance value at the border to the anchizone is assumed to be 4%, a value not reached by even the deepest sample of the Mikulov Formation. This inference is supported by illite crystallinity data that show that even the deepest samples (8500 m) are still in the diagenetic zone (Fig. 7).

5.3. The Mikulov formation as a potential unconventional play-seen from a mineralogical and pore type point of view

Successful unconventional shale gas and shale oil plays require the interaction of a number of parameters. These include source rock composition and richness, organic matter type, thickness, quality and maturity of the shale as well as gas-in-place and production efficiency (Bernard et al., 2010).

This study concentrates on the mineralogical composition of a source rock which is an important factor as it controls the brittleness of the rock and thus its mechanical behaviour with regard to hydraulic fracturing. In the well-established Barnett shale play, it is the high diagenetic quartz content that contributes to the brittleness of the shale (Fig. 4). X-ray diffraction studies show an equal amount of quartz and clay minerals of 35% on average and only subordinate amounts of carbonate and pyrite (Rowe et al., 2008; Ruppel and Loucks, 2008). In another well studied shale reservoir, the Eagle Ford Shale (Fig. 4), calcite, rather than quartz dominates cementation within the reservoir (Schieber et al., 2016), suggesting that calcite cementation might also be an important factor for potential reservoir facies. Besides, for successful stimulation, a favourable reservoir rock for shale gas or oil production should contain less than 50% clay minerals (Bowker, 2007). In the Mikulov Formation the amount of clay in the bulk samples ranges between 14 and 46 vol% and thus looks favourable. However, the actual amount of quartz cement is low. Here, the carbonates are the dominant non-clay mineral, and have the potential to enhance mechanical strength through cementation, as well as preserving porosity (Schieber et al., 2016) (Fig. 4).

Aside of bulk mineralogy, the composition of the clay fraction is another important factor that controls the unconventional hydrocarbon potential (Sliwinski et al., 2010). Particularly, large amounts of expandable clays (e.g. smectite) have a negative effect on hydraulic fracturing success. According to Rupprecht et al. (2017), at around 5500 m depth a vitrinite reflectance of 1.3% R_o for the Mikulov Formation is reached. This is considered to be the cut-off value for economic shale gas production. Based on our mineralogical analyses, below a depth of 4500 m expandable smectite ranges between 0.3 and 3.8% in bulk samples of the Mikulov Formation which would be favourable for shale gas exploration (Table 2, Fig. 11).

Looking at the mudstones of the Mikulov Formation at the micrometer and nanometer scale provides further insights into the reservoir potential of these rocks. Multiple pore types of micrometer to nanometer size are encountered in almost all samples (Fig. 10 b,d,f,j,k,l,m,n,p), reflecting the depositional, diagenetic, and catagenic history of the Mikulov Formation. SEM photomicrographs cannot be used to establish whether these various pores are interconnected, but most likely they collectively contribute to the effective porosity and permeability of these rocks. Observed pore types include phyllosilicate framework pores, carbonate framework pores, organic matter pores and secondary pores due to dissolution of carbonates, an association that is common to many shale reservoirs (e.g. Schieber, 2013; Schieber et al., 2016). In addition, fractures (Fig. 3c) of mm-size, partly lined with calcite cement occur naturally and contribute to permeability.

Some properties, such as the overall thickness, limited presence of expandable clay minerals and the presence of pores, are favourable for the Mikulov Formation as an unconventional play. Others, however, like geomechanical properties, warrant further investigation. Rupprecht et al. (2017) evaluated the organic parameters of the mudstones of the Mikulov Formation. They concluded that based on TOC contents (typically <2.0 wt%) and primarily the rather deep position of the maturity cut-off values required for unconventional hydrocarbon production (~4000 m for shale oil and ~5000 m for shale gas), the economic potential of the Mikulov Formation as an unconventional hydrocarbon play is very limited.

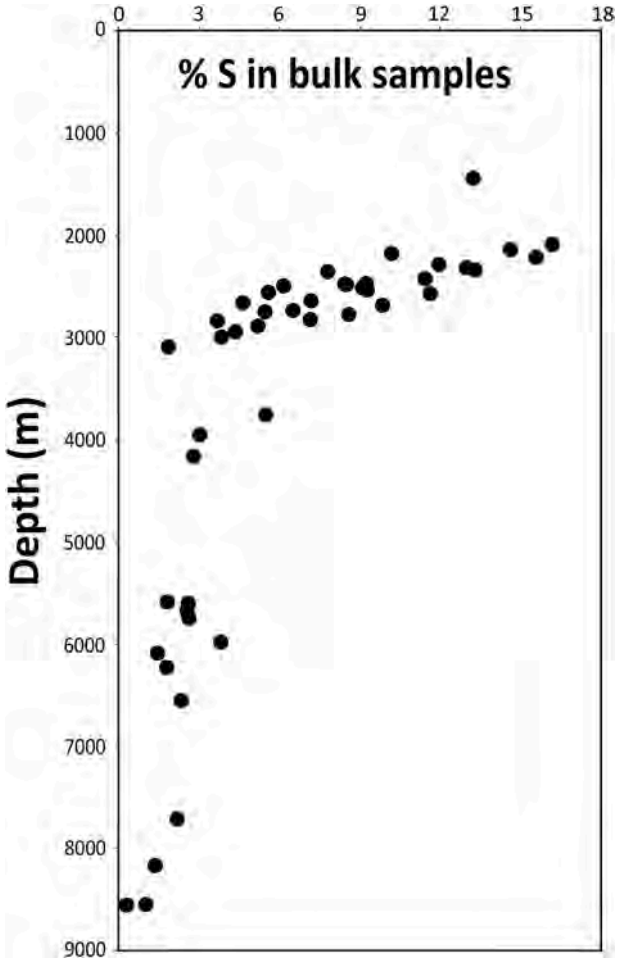

Fig. 11. % Smectite (S) in bulk samples.

6. Conclusions

Based on maturity data, the theoretical zone of interest for shale gas exploration in the Vienna Basin is below 5000 m; there, the bulk samples contain only 0.3–3.8% smectite. The window for economic shale gas production currently puts the Mikulov Formation at an uneconomic depth.

The Illitization of smectite with depth provided ions for a variety of late diagenetic mineral cements, which resulted for instance in quartz overgrowths and ankerite cements in the matrix. The transition from random to ordered mixed-layering occurs at a depth of approximately 2800 m and a vitrinite reflectance of 0.4%–0.6%. Diagenesis did not only result in formation of cements, but also in development of multiple types of nanometer to micrometer size pores that are an integral part of the depositional, diagenetic, and catagenic history of these rocks. Although SEM photomicrographs do not provide direct evidence of interconnectedness of these pores, collectively they most likely contributed to the overall effective porosity and permeability and the reservoir potential of these rocks.

Credit author statement

Andrea Schicker performed most of the analyses as part of her PhD thesis and wrote the manuscript. Susanne Gier supervised the thesis, did some of the analyses, helped with interpretation, discussed the results and wrote the manuscript. Jürgen Schieber did the SEM analyses on ion milled surfaces and helped with thin section interpretation. Peter Krois wrote the Geology part of the manuscript and helped with petroleum geology context.

Declaration of competing interest

The authors declare that they have no known competing financial interests or personal relationships that could have appeared to influence the work reported in this paper.

Acknowledgments

The authors thank OMV Exploration & Production for providing the material and for permission to publish this work. Thanks also to the staff at the University of Vienna and at the University of Life Sciences in Vienna for discussions and helping with sample preparations. A National Science Foundation equipment grant to J. Schieber (EAR-0318769) provided funds for the purchase of the analytical scanning electron microscope that was used to acquire some of the data and images for this article. Richard Worden is thanked for his valuable comments and suggestions which helped to improve the manuscript. Two anonymous reviewers and the Journal Editor are thanked for their work.

Appendix A. Supplementary data

Supplementary data to this article can be found online at https://doi.org/10.1016/j.marpetgeo.2021.105082.

References

Arzmüller, G., Buchta, Š., Ralbovský, E., Wessely, G., 2006. The Vienna Basin. In: Golonka, J., Picha, F.J. (Eds.), The Carpathians and Their Foreland: Geology and Hydrocarbon Resources, vol. 84. AAPG Memoir, pp. 191–204.

Asala, H., Ahmadi, M., Taleghani, A.D., 2016. Why re-fracturing works and under what conditions, SPE-181516-MS. In: SPE Annual Technical Conference & Exhibition, 26 September – 28 September, Dubai, UAE. https://doi.org/10.2118/181516-MS.

Bernard, S., Horsfield, B., Schulz, H.-M., Schreiber, A., Wirth, R., Thianhvu, T., Perssen, F., Könitzer, S., Volk, H., Sherwood, N., Fuentes, D., 2010. Multi-scale detection of organic and inorganic signatures provides insights into gas shale properties and evolution. Chem. Erde 70 (S3), 119–133.

Boles, J.R., Franks, S.G., 1979. Clay diagenesis in Wilcox sandstones of southwest Texas: implications of smectite diagenesis on sandstone cementation. J. Sediment. Petrol. 49, 55–70.

Bowker, K.A., 2007. Barnett shale gas production, fort worth basin: issues and discussion. AAPG (Am. Assoc. Pet. Geol.) Bull. 91, 523–533.

Day-Stirrat, R.J., Milliken, K.L., Dutton, S.P., Loucks, R.G., Hillier, S., Aplin, A.C., Schleicher, A.M., 2010. Open-system chemical behavior in deep Wilcox group mudstones, Texas gulf coast, USA. Mar. Petrol. Geol. 27, 1804–1818.

Decker, K., Peresson, H., 1996. Tertiary kinematics in the Alpine-Carpathian-Pannonian system: links between thrusting, transform faulting and crustal extension. In: Wessely, G., Liebl, W. (Eds.), Oil and Gas in Alpidic Thrustbelts and Basins of Central and Eastern Europe, vol. 5. EAGE Special Publication, pp. 69–77.

DIN 51033, 1962. Prüfung keramischer Roh- und Werkstoffe, Bestimmung der Korngrößen durch Siebung und Sedimentation, Verfahren nach Andreasen.

Dowey, P.J., Taylor, K.G., 2017. Extensive authigenic quartz overgrowths in the gasbearing Haynesville-Bossier Shale, USA. Sediment. Geol. 356, 15–25.

Dowey, P.J., Taylor, K.G., 2019. Diagenetic mineral development within the upper jurassic haynesville-bossier shale, USA. Sedimentology. https://doi.org/10.1111/sed.12624.

Dunham, R.J., 1962. Classification of carbonate rocks according to depositional texture. In: Ham, W.E. (Ed.), Classification of Carbonate Rocks: AAPG Memoir 1, pp. 108–121.

Eliáš, M., Wessely, G., 1990. The autochthonous Mesozoic on the eastern flank of the Bohemian Massif - an object of mutual geological effort between Austria and CSSR. In: Minacikova, D., Lobitzer, H. (Eds.), Thirty Years of Geological Cooperation between Austria and Czechoslovakia, vol. 78. Federal Geological Survey Vienna and Geological Survey Prague, p. 83.

Franců, J., Müller, P., Šucha, V., Zatkalíková, V., 1990. Organic matter and clay minerals as indicators of thermal history in the Transcarpathian depression (East Slovakian Neogene basin) and the Vienna Basin. Geol. Carpathica 41, 535–546.

Gier, S., 1998. Burial diagenetic processes and clay mineral formation in the Molasse Zone of Upper Austria. Clay Clay Miner. 46, 658–669.

Gier, S., 2000. Clay mineral and organic diagenesis of the lower Oligocene Schöneck fishshale, western Austrian molasse basin. Clay Miner. 35, 709–717.

Glover, E.D., 1961. Method of solution of calcareous materials using the complexing agent, EDTA. J. Sediment. Petrol. 31, 622–626.

Granado, P., Ferrer, O., Munoz, J.A., Thöny, W., Strauss, P., 2017. Basin inversion in tectonic wedges: insights from analogue modeling and the Alpine-Carpathian fold-and-thrust belt. Tectonophysics 703 – 704, 50–68.

Hillier, S., Mátyás, J., Matter, A., Vasseur, G., 1995. Illite/smectite diagenesis and its variable correlation with vitrinite reflectance in the Pannonian Basin. Clay Clay Miner. 43, 174–183.

Horton, R.B., Johns, W.D., Kurzweil, H., 1985. Illite diagenesis in the Vienna Basin, Austria. Tschermaks Mineral. Petrogr. Mittl. 34, 239–260.

Hower, J., Eslinger, E.V., Hower, M.E., Perry, E.A., 1976. Mechanism of burial metamorphism of argillaceous sediment: 1. Mineralogical and chemical evidence. Geol. Soc. Am. Bull. 87, 725–737.

Hu, Z., Qi, L., 2014. 15.5. Sample digestion methods. In: Turekian, K., Holland, H. (Eds.), Treatise on Geochemistry, second ed. Elsevier, Oxford, pp. 87–109. 2014.

Jarvie, D.M., Hill, R.J., Ruble, T.E., Pollastro, R.M., 2007. Unconventional shale-gas systems: mississippian Barnett Shale of north-central Texas as one model for thermogenic shale-gas assessment. AAPG (Am. Assoc. Pet. Geol.) Bull. 91, 475–499.

Johns, W.D., Kurzweil, H., 1979. Quantitative estimation of illite-smectite mixed-phases formed during burial diagenesis. Tschermaks Mineral. Petrogr. Mittl. 26, 203–215.

Kisch, H.J., 1987. Correlation between indicators of very low-grade metamorphism. In: Frey, M. (Ed.), Low Temperature Metamorphism. Blackie, Glasgow, pp. 227–300.

Köster, H.M., 1977. Die Berechnung kristallchemischer Strukturformeln von 2:1-Schichtsilikaten unter der Berücksichtigung der gemessenen Zwischenschichtladungen und Kationenumtauschkapazitäten, sowie die Darstellung der Ladungsverteilung in der Struktur mittels Dreieckskoordinaten. Clay Miner. 12, 45–54.

Köster, H.M., 1982. The crystal structure of 2:1 layer silicates. In: Van Olphen, H., Veniale, F. (Eds.), Developments in Sedimentology 35, International Clay Conference 1981. Elsevier, p. 41.

Kröll, A., Wessely, G., 1973. Neue Ergebnisse beim Tiefenaufschluß im Wiener Becken. Erdol Erdgas Z 89, 400–413.

Kroner, U., Mansy, J.L., Mazur, S., Aleksandrowski, P., Hann, H.P., Huckriede, H., 2008. Variscan tectonics. In: McCann, T. (Ed.), The Geology of Central Europe: Vol. 1 Precambrian and Paleozoic. Geological Society London, pp. 665–712.

Kurzweil, H., Johns, W.D., 1981. Diagenesis of tertiary marlstones in the Vienna Basin. Tschermaks Mineral. Petrogr. Mittl. 29, 103–125.

Ladwein, H.W., 1988. Organic geochemistry of Vienna Basin: model for hydrocarbon generation in overthrust belts. AAPG (Am. Assoc. Pet. Geol.) Bull. 72, 586–599.

Lazar, O.R., Bohacs, K.M., Macquaker, J.H.S., Schieber, J., Demko, T.M., 2015. Capturing key attributes of fine-grained sedimentary rocks in outcrops, cores, and thin sections: nomenclature and description guidelines. J. Sediment. Res. 85, 230–246.

Marfil, R., Delgado, A., Rossi, C., La Iglesia, A., Ramseyer, K., 2003. Origin and diagenetic evolution of kaolin in reservoir sandstones and associated shales of the Jurassic and Cretaceous, Salam Field, Western Desert (Egypt). In: International Association of Sedimentologists Special Publication, vol. 34, pp. 319–342.

McKinley, J.M., Worden, R.H., Ruffell, A.H., 2003. Smectite in sandstones: a review of the controls on occurrence and behaviour during diagenesis. In: Worden, R.H., Morad, S. (Eds.), Clay Mineral Cements in Sandstones, vol. 34. International Association of Sedimentologists, Special Publications, pp. 109–128.

Marshall, C.E., 1949. The structural interpretation of chemical analyses of the clay minerals. In: The Colloid Chemistry of the Silicate Minerals. Academic Press, New York, p. 159.

Merriman, R.J., Frey, M., 1999. Patterns of very low-grade metamorphism in metapelitic rocks. In: Frey, M., Robinson, D. (Eds.), Lowgrade Metamorphism. Blackwell, Oxford, pp. 61–107.
Meunier, A., 2005. Clays. Springer, Berlin, Heidelberg, p. 472.
Milan, G., Sauer, R., 1996. Ultra-deep drilling in the Vienna Basin – a review of geological results. In: Wessely, G., Liebl, W. (Eds.), Oil and Gas in Alpidic Thrustbelts and Basins of Central and Eastern Europe, vol. 5. EAGE Special Publication, pp. 109–117.
Moore, D.M., Reynolds Jr., R.C., 1997. X-ray Diffraction and the Identification and Analysis of Clay Minerals. Oxford University Press, New York, p. 378.
Morse, J.W., Wang, Q., 1997. Pyrite formation under conditions approximating those in anoxic sediments: II. Influence of precursor iron minerals and organic matter. Mar. Chem. 57, 187–193.
Peltonen, C., Marcussen, Ø., Bjørlykke, K., Jahren, J., 2009. Clay mineral diagenesis and quartz cementation in mudstones: the effects of smectite to illite reaction on rock properties. Mar. Petrol. Geol. 26, 887–898.
Perry, E., Hower, J., 1970. Burial diagenesis in Gulf Coast pelitic sediments. Clay Clay Miner. 18, 165–177.
Rowe, H.D., Loucks, R.G., Ruppel, S.C., Rimmer, S.M., 2008. Mississippian Barnett formation, fort worth basin, Texas: bulk geochemical inferences and Mo–TOC constraints on the severity of hydrographic restriction. Chem. Geol. 257, 16–25.
Royden, L.H., 1985. The Vienna Basin: a thin-skinned pull-apart basin. In: Biddle, K.T., Christie-Blick, N. (Eds.), Strike-slip Deformation, Basin Formation and Sedimentation, vol. 37. SEPM Spec. Publ., pp. 319–338
Ruppel, S.C., Loucks, R.G., 2008. Black mudrocks: lessons and questions from the mississippian Barnett shale in the southern midcontinent. Sediment. Rec. 6 (2), 4–8.
Rupprecht, B.J., Sachsenhofer, R.F., Gawlick, H.-J., Kallanxhi, M.-E., Kucher, F., 2017. Jurassic source rocks in the Vienna Basin (Austria): assessment of conventional and unconventional petroleum potential. Mar. Petrol. Geol. 86, 1327–1356.
Sachsenhofer, R.F., 2001. Syn- and post-collisional heat flow in the cenozoic eastern Alps. Int. J. Earth Sci. 90, 579–592.
Sachsenhofer, R.F., Rantitsch, G., Hasenhüttl, C., Russegger, B., Jelen, B., 1998. Smectite to illite diagenesis in early Miocene sediments from the hyperthermal western Pannonian Basin. Clay Miner. 33, 523–537.
Sauer, R., Seifert, P., Wessely, G., 1992. Guidebook to excursions in the Vienna Basin and the adjacent alpine-carpathian thrustbelt in Austria. Mittl. Osterreichischen Geol. Ges. 85, 1–264.
Schieber, J., 2010. Common Themes in the Formation and Preservation of Intrinsic Porosity in Shales and Mudstones—Illustrated with Examples across the Phanerozoic: Society of Petroleum Engineers Unconventional Gas Conference, Pittsburgh, Pennsylvania, February 23–25, 2010, p. 10. https://doi.org/10.2118/132370-MS. SPE Paper 132370.
Schieber, J., 2011. Marcasite in black shales-a mineral proxy for oxygenated bottom waters and intermittent oxidation of carbonaceous muds. J. Sediment. Res. 81, 447–458.
Schieber, J., 2013. SEM observations on Ion-milled samples of Devonian Black Shales from Indiana and New York: the petrographic context of multiple pore types. In: Camp, W., Diaz, E., Wawak, B. (Eds.), Electron Microscopy of Shale Hydrocarbon Reservoirs: AAPG Memoir, vol. 102, pp. 153–172.
Schieber, J., Krinsley, D., Riciputi, L., 2000. Diagenetic origin of quartz silt in mudstones and implications for silica cycling. Nature 406, 981–985.
Schieber, J., Lazar, R., Bohacs, K., Klimentidis, B., Dumitrescu, M., Ottmann, J., 2016. An SEM study of porosity in the Eagle Ford Shale of Texas— pore types and porosity distribution in a depositional and sequence stratigraphic context. In: Breyer, J.A. (Ed.), The Eagle Ford Shale: A Renaissance in U.S. Oil Production: AAPG Memoir 110, pp. 167–186.
Schmid, S.M., Fügenschuh, B., Kissling, E., Schuster, R., 2004. Tectonic map and overall architecture of the Alpine orogen. Eclogae Geol. Helv. 97, 93–117.
Schultz, L.G., 1964. Quantitative interpretation of mineralogical composition from X-ray and chemical data for the Pierre shale. *US Geol Survey Prof Paper*, 391-C, Washington.
Seifert, P., 1996. Sedimentary-tectonic development and Austrian hydrocarbon potential of the Vienna Basin. In: Wessely, G., Liebl, W. (Eds.), Oil and Gas in Alpidic Thrustbelts and Basins of Central and Eastern Europe, vol. 5. EAGE Special Publication, pp. 331–341.
Sliwinski, J., Harrington, J., Power, M., Hughes, P., Yeung, B., 2010. A high-definition mineralogical examination of potential gas shales. Search and Discovery Article #50290. AAPG, New Orleans (11-14 April 2010).
Środoń, J., 1999. Nature of mixed-layer clays and mechanisms of their formation and alteration. Annu. Rev. Earth Planet Sci. 27, 19–53.
Środoń, J., Kotarba, M., Biroň, A., Such, P., Clauer, N., Wójtowicz, A., 2006. Diagenetic history of the Podhale-Orava Basin and the underlying Tatra sedimentary structural units (Western Carpathians): evidence from XRD and K-Ar of illite-smectite. Clay Miner. 41, 751–774.
Tanner, C.B., Jackson, M.L., 1948. Nomographs of sedimentation times for soil particles under gravity or centrifugal acceleration. Soil Sci. Soc. Am. J. 12, 60–65.
Thyberg, B., Jahren, J., 2011. Quartz cementation in mudstones: sheet-like quartz cement from clay mineral reactions during burial. Petrol. Geosci. 17, 53–63.
Van de Kamp, P.C., 2016. Potassium distribution and metasomatism in pelites and schists: how and when, relation to postdepositional events. J. Sediment. Res. 86, 683–711.
Velde, B., Lanson, B., 1993. Comparison of I/S transformation and maturity of organic matter at elevated temperatures. Clay Clay Miner. 41, 178–183.
Wagreich, M., Schmid, H.P., 2002. Backstripping dip-slip fault histories: apparent slip rates for the Miocene of the Vienna Basin. Terra. Nova 14, 163–168.
Warr, L.N., Rice, A.H.N., 1994. Interlaboratory standardization and calibration of clay mineral crystallinity and crystallite size data. J. Metamorph. Geol. 12, 141–152.
Welton, J.E., 1984. SEM Petrology Atlas. Methods in Exploration Series. The American Association of Petroleum Geologists, Tulsa, Oklahoma, p. 237p.
Wessely, G., 1987. Mesozoic and Tertiary evolution of the Alpine-Carpathian foreland in eastern Austria. Tectonophysics 137, 45–49.
Wessely, G., 2006. Niederösterreich, Geologie der österreichischen Bundesländer. Geologische Bundesanstalt, Wien, p. 416.
Zimmer, W., Wessely, G., 1996. Exploration results in thrust and sub-thrust complexes in the Alps and below the Vienna Basin in Austria. In: Wessely, G., Liebl, W. (Eds.), Oil and Gas in Alpidic Thrustbelts and Basins of Central and Eastern Europe, vol. 5. EAGE Special Publication, pp. 81–107.